Atmos. Chem. Phys. Discuss., https://doi.org/10.5194/acp-2018-225
Manuscript under review for journal Atmos. Chem. Phys.
Discussion started: 25 April 2018

Atmospheric Chemistry and Physics Discussions

Air quality in the middle and lower reaches of the Yangtze River channel: A cruise campaign

Zhong Li[1], Chunlin Li[1,2], Xingnan Ye[1], Hongbo Fu[1], Lin Wang[1], Xin Yang[1], Xinke Wang[3], Zhuohui Zhao[4], Haidong Kan[4], Abdelwahid Mellouki[5], Jianmin Chen[1,4,*]

[1] *Shanghai Key Laboratory of Atmospheric Particle Pollution and Prevention, Fudan Tyndall Center, Department of Environmental Science & Engineering, Institute of Atmospheric Sciences, Fudan University, Shanghai 200433, China*

[2] *Department of Earth and Planetary Sciences,Weizmann Institute of Science*

[3] *Univ Lyon, Université Claude Bernard Lyon 1 CNRS, IRCELYON, F-69626, Villeurbanne, France*

[4] *School of Public Health, Fudan University, Shanghai 200032, China*

[5] *Institut de Combustion, Aérothermique, Réactivité et Environnement, CNRS, 45071 Orléans cedex 02, France*

[*]**Correspondence to:** Jianmin Chen (jmchen@fudan.edu.cn)

Atmos. Chem. Phys. Discuss., https://doi.org/10.5194/acp-2018-225
Manuscript under review for journal Atmos. Chem. Phys.
Discussion started: 25 April 2018

Atmospheric Chemistry and Physics Discussions

Abstract

Yangtze River is the longest river in China, nearly one-third of the national population lives along the River. Air quality over the Yangtze River is interesting as it may have significant influences on aquatic ecosystem, public health onboard and coastal areas. A comprehensive15-days cruise campaign has been performed in the Mid-Lower Reaches Yangtze River (MLYR) in winter of 2015. Based on the filter samples, the concentration and chemical composition of $PM_{2.5}$ were greatly varied or fluctuated in different regions. Crustal elements (Ca, Mg, Al and K) from floating dust showed peak concentrations in the Yangtze River Delta (YRD) regions, while secondary species (SO_4^{2-}, NO_3^- and NH_4^+) and some most enriched elements (Pb, As, Se and Cd) presented high levels in the central China (Wuhan). The significant correlation between Se and SO_4^{2-} suggested that coal combustion may play a key role on the secondary inorganic formation. The relative high enrichment factors (EFs) of Ca (EFs > 100) suggested the crustal elements may derive from anthropogenic sources. Furthermore, the concentration of levoglucosan in $PM_{2.5}$ and CO column level from satellite data greatly enhanced in the rural area (Anhui and Jiangxi), indicating that biomass burning may make remarkable contribution to rural area. The concentrations of V and Ni were found to evidently elevate in the Shanghai port, which were mainly ascribed to the ship emission through the air mass source analysis and the relatively high ratio of V/Ni as well. This result shown herein portrayed a good picture of air pollution along the Yangtze River.

Keywords:

Shipboard observation, chemical composition, ship engine emission, Mid-Lower Yangtze Plain

1 Introduction

The Yangtze river is the longest river in China, originating from the Qinghai-Tibetan Plateau and extending to the East China Sea, and it drains an area of 18,08,500 square km basin, of which is China's great granary and contains nearly one-third of the national population (Liu et al., 2007; Xiang et al., 2002; Jiang et al., 2008). Along both shores of the Mid-Lower Reaches Yangtze River (MLYR), there are main composed of three city agglomerations, including Wuhan, Nanjing and Shanghai, which are the centers of economy, politics, and culture in the

Middle and Eastern China, all of which are home to larger petrochemical complex and/or steel industry. MLYP is one of the most developed and economically vibrant regions in China, accounting for 34.13% of China's total GDP in 2015. Owing to fast economic development and industrialization, the MLYP region has become one of the most polluted areas in China (Xu et al., 2016b).

Physical properties and chemical compositions of fine aerosol particles are becoming more important in recently years, due to their effects on human health, agriculture, and climate change (Wang et al., 2012;Kang et al., 2013a;Pöschl, 2005;Seaton et al., 1995;Ackerman et al., 2004;Stier et al., 2005;Chameides et al., 1999;Novakov and Penner, 1993;Jones et al., 1994). Numerous field researches related to fine particle have been conducted in megacities of the Yangtze River Delta (YRD) region. At present, the fine particle concentrations, chemical compositions, size distributions, seasonal variations, daily change optical properties and possible sources in this region have been generally characterized (Zhou et al., 2016;Kang et al., 2013a;Tao et al., 2014b;Shen et al., 2014;Fu et al., 2014;Huang et al., 2013;Huang et al., 2012b;Huang et al., 2012a;Ding et al., 2013a;Ding et al., 2017;Zhang et al., 2010). By analysis of several serious haze cases, Huang et al. (2012) pointed out that secondary inorganic species (SNA, SO_4^{2-}, NO_3^- and NH_4^+) and dust pollution erupted in spring, while biomass burning (BB) event was often observed in summer (harvest season for wheat). The high values for sulfate oxidizing rate (SOR) and nitrate oxidizing rate (NOR) were also observed from long-term field measurements in Nanjing and Shanghai, indicating that atmospheric photochemical processes were quit active in these areas (Zhou et al., 2016;Zhou et al., 2017;An et al., 2015). Wang et al. (2015b) also found that secondary inorganic species highly contributed to the $PM_{2.5}$ pollution. Additionally, the increase trend of the NO_3^-/SO_4^{2-} ratio suggested that vehicle sources became more and more important (Kang et al., 2013b;Huang et al., 2012a;Tao et al., 2014b). Beyond, Cheng et al. (2014) estimated that BB contributed to 37% of $PM_{2.5}$, 70% of organic carbon and 61% of element carbon in harvest, respectively. If BB was controlled and even forbidden, the $PM_{2.5}$ level would decrease by 47% in the YRD region (Cheng et al., 2014). Some typical events, including fresh combustion pollution from firework (Zhang et al., 2010;Kong et al., 2015), and

peaking SNA originated from travel rush and re-opening of factories after China Spring Festival (Huang et al., 2012b;Kong et al., 2015) have also focused and analyzed. Huang et al. (2013) found that the concentration of anthropogenic Ca decreased as results of implementing strict emission control of construction activity during 2010 Word Expo. During the 2014 Youth Olympic Games (YOG), the levels of Ca^{2+} and SO_2 reduced 55% and 46%, respectively (Zhou et al., 2017).

The MLYR faces the most complex anthropogenic emission sources effecting its air quality, including a variety of power plants, large petrochemical and steel industries, and farmland located on both banks of the Yangtze River, as well as ship emission. It was well documented that ship emissions displayed a significant impact on regional air quality, particularly in traffic hubs and harbors (Pandis et al., 1999;Becagli et al., 2017;Zhan et al., 2014). The contribution and effect of ship-plume to local air pollution, especially particulate matter, have been partly analyzed in global and regional scale (Jalkanen et al., 2015;Zhan et al., 2014;Pandis et al., 1999;Fan et al., 2016;Coggon et al., 2012). The emission factors and properties of emitted particles and gases from ship plume in different engine speeds were also reported (Zhang et al., 2016;Moldanová et al., 2009;Agrawal et al., 2009). Ship-related pollutants have been identified in the YRD port cluster and surrounding areas. In 2010, the ship emissions of SO_2, NO_x and $PM_{2.5}$ in this region were 3.8×10^5 t/y, 7.1×10^5 t/y and 5.1 × t/y, respectively. The maximal SO_2 and NOx concentrations from ship in harbors or traffic hubs were nearly 36 times and 17 times higher than the maximal land-based emissions, respectively (Fan et al., 2016). Zhao et al. (2013b) noted that Ni and V enriched in fine particles in Shanghai port. Recently, Liu et al. (2017) reported that ship plume contributed to 2-7 μg m^{-3} to fine particle within the coastal of Shanghai port, accounting for 20-30% of total $PM_{2.5}$. Known as “golden canal”, Yangtze River was an important route of trade and travel. However, there is seldom data related to air quality and the influence of ship emission along the Yangtze River channel. Meanwhile, related observations for synchronous trend of aerosol in the MLYP region remain insufficient.

To characterize the air quality in this region, a comprehensive field observation, namely Yangtze River Campaign (YRC), was conducted from 22 November to 05 December 2015

along the Yangtze River. Multitudinous off-line and online instruments were installed on a vessel and a round-trip observation voyage was carried out from Shanghai to Wuhan. The purpose of this cruise campaign was main to characterize the components of atmospheric pollutants, to analyze their spatial distribution, and to identify their potential sources. Herein, the data of the gaseous pollutants (SO_2, CO, O_3, NO-NO_X), meteorological parameters and the satellite data in this region were also collected and analyzed. Back trajectory, principle component analysis (PCA) and potential source contribution functions (PSCF) were applied to determine the potential geographic distribution of fine particles and their main sources over the MLYP region during the cruise. To the best of our knowledge, it is the first systematic observation to characterize the air pollution along the China's largest and longest river.

2 Measurements and methods

2.1 Overview YRC

A mobile haze monitoring platform (A container: length 10 m, width 4 m and height 2.5m) was placed on the vessel (length: 20 m, width 6 m), sailing from 22 November to 05 December in 2015 along the Yangtze River channel between Shanghai to Wuhan (29.72˚N-32.33˚N, 114.33˚E-121.61˚E). This campaign route was illustrated in Figure 1. Starting on 22 November in the Waigaoqiao port of Shanghai, then the vessel crossed Jiangsu, Anhui province and finally arrived at the Hankou port in Wuhan, Hubei province on 29 November along the Yangtze River waterway. The ship shifted at an average speed of 1 m/s heading the upper the Yangtze River towards Wuhan. After berthing in the port of Wuhan one night, the vessel turned around, departed and proceeded towards Shanghai. This cruise finally ended in the Waigaoqiao port in Shanghai on 5 December. During YRC, a wide range of data, including common meteorological parameters, trace gas concentrations (CO, NO-NO_x, SO_2 and O_3), were acquired. The aerosol particles were collected on the filter samples for chemical composition analysis.

2.2 Trace gases measurements

A set of commercial trace gas instruments (Thermo Environmental Instruments Ins., USA C-series), including 43i SO_2 analyzer, 49i O_3 analyzer, 48i CO analyzer, and 42i NO-NO_2-NO_x analyzer, were installed in an air-conditioned container to measure gaseous pollutants. The

routine QA/QC (the daily zero/standard calibration) procedures were followed the technical guidance established by U.S. Environmental Protection Agency (USEPA, 1998).

Trace alkanes, including toluene and benzene, were also sampled in stainless summa canister and quantified by a gas chromatograph with a mass spectrometer and a flame ionization detector (GC-MS/FID) (Wang et al., 2014). The sampling time of VOCs was 3 hours with fluctuation. The ratio of toluene/benzene (T/B) was commonly regarded as an indicator of the photochemical age (Baltrenas et al., 2011). The high ratio of T/B indicated that air masses were fresh emission, while lower value suggested that air masses had undergone photochemical processes. In this paper, we used the same value ratio of T/B in CalNex (Gaston et al., 2013). Air masses with T/B << 1 were excepted to well undergo photochemical aging while urban fresh air masses had much higher T/B ratio ($\geqslant$2). Ship track self-emission was removed by subducting the periods when the wind blew from the stern, that is, the relative wind direction was from 130˚ to 220˚ to the ship direction (0˚ in the front). The real-time measurement of trace gases and aerosol data presented here were all filtered out by this method.

2.3 Chemical analysis of the filter samples

The filter samples of $PM_{2.5}$ and $PM_{1.0}$ were collected on the separate quartz filters (Φ90 mm, Whatman Inc., Maidstone, UK) using a medium-volume sampler by HY-100 (Qingdao Hengyuan S.T. Development Co., Ltd, China) (model: $PM_{2.5}/PM_{1.0}$; flow rate: 100 L min^{-1}), which was placed on the foredeck about 3 meters above sea levels. The sampling time was generally set at 12 h (in parallels: day 07:00-19:00, night 19:00-07:00), while it was also collected PM for 24 h. The quartz filters were preheated at 500 ℃ for 10 h to remove the residues prior to sampling. All the samples were stored in a refrigerator at -20 ℃ for analysis. The particle masses were measured by an intelligent weight system (Hangzhou Wmade Intelligent Technology co., LTD) after the equilibration at 20 ℃ for 24 h under RH of 40%. All of the procedures were strictly controlled to avoid the possible contamination. The sample instrument was placed on the bow of the ship far away of its track. Ship self-emission in the

filter samples was ignored since the most prevailing winds blew from the bow to the stern during the sampling.

One-eighth of each filter was extracted ultrasonically by 20 mL of deionized water for 40 min (18.2 MΩ cm^{-1}). After filtering, eight inorganic ions (SO_4^{2-}, NO_3^-, Cl^-, NH_4^+, Na^+, K^+, Ca^{2+}, and Mg^{2+}) were analyzed by an ion chromatography (940 Professional IC, Metrohm, Switzerland) and a sugar column (945 Professional Detector Vario, Metrohm, Switzerland) was used to measure levoglucosen by the high-performance anion-exchange chromatography coupled with pulsed electrochemical detection (HPAEC-PAD) method in the extract. Both of instruments were controlled with a 940 Professional IC software. The lower and upper limits of the detection were 0.5 and 4 μg m^{-3}, respectively. The relative standard deviation of each ion was < 2% from three reproducibility tests. Six blank samples were analyzed with the same processes to remove possibly contaminations.

One-eighth of the sample filter and the blank filter were cut into fragment and digested at 170 °C for 4 h in a high pressure Teflon digestion vessel with 3 mL of HNO_3 and 1 mL of $HClO_4$ (Wang et al., 2006;Li et al., 2015b). After cooling, the digested solution was filtered and diluted to 15 mL with less than 2% acidity with ultrapure Mill-Q water. An inductively coupled plasma mass spectrometer (ICP-MS, Agilent 7500a) was employed to measure the concentrations of 17 elements (Al, As, Ca, Co, Cr, Cu, Fe, K, Mg, Mn, Na, Ni, Se, Tl, Pb, V and Zn) in the samples. National standard material (soil, GSS-12, China) was digested and applied to calculate the element recoveries ranging from 91%-102%. The detection limits of the trace elements were derived from the standard deviation (3δ) of the blank values. Details relating to ICP-MS have been described (Li et al., 2015b).

Organic carbon (OC) and elemental carbon (EC) in the aerosol samples were analyzed by a Thermal/Optical Carbon Analyzer (DRI Model 2001). Each sample was identified as four OC fraction (OC1, OC2, OC3, and OC4 at 120, 250, 450, and 550 °C, respectively in a helium air) and three EC fraction (EC1, EC2, EC3 at 550,700 and 800 °C, respectively, in the mixture air (98% helium and 2% oxygen) by an IMPROVE thermal/optical reflectance (TOR) protocol.

Pyrolyzed organic carbon (POC) was separately detected by transmittance. IMPROVE OC was defined as OC1 + OC2 + OC3 + OC4 + POC and EC was calculated by EC1 + EC2 + EC3 − POC.

2.4 Satellite data and ship traffic data

The satellite databases, including Moderate Resolution Imaging Spectroradiometer (MODIS), Measurement of Pollutants in the Troposphere (MOPITT) and Ozone Monitoring Instrument (OMI) on the National Aeronautics and Space Administration's Earth Observing System (NASA's EOS) Aura satellite, were applied to provide spatial distribution of aerosol particles and trace gases (Xu et al., 2011;Huang et al., 2012a). The column levels of CO, NO_2, SO_2 and aerosol optical depth (AOD) at 550 nm were retrieved over the MLYP region. Considering different conditions for databases, the poor-quality data was removed.

Ship positions and numbers in the Yangtze River channel were decoded by Automatic Identification System (AIS) database which was obtained from the Marine Department. A 15-day AIS data set in the region of MLYP was chosen with a high time resolution (about 15min).

2.5 Potential source contribution function

The potential source contribution function developed by Hopke et al. (1995) was applied to derive the potential source regions and spatial distribution. In this study, 3 days back trajectories at arrival height 500 m was computed using National Oceanic and Atmospheric Administration (NOAA) Hybrid Single Particle Lagrangian Integrated Trajectory (HYSPLIT-4) model (http://www.arl.noaa.gov/ready/open/hysplit4.html) with global meteorological data from NCEP Reanalysis data (ftp://arlftp.arlhq.noaa.gov/pub/archives/reanalysis) (Draxler and Hess, 1998). The contribution of potential source during YRC was calculated by the PSCF analysis with TrajStat (Wang et al., 2009). The domain sources were restricted to 25°N-45°N and 110°E-125°E, which were divided into grid cells with a 0.5°×0.5° resolution. The PSCF value for the *ij* th grid cell was defined as:

$$\mathrm{PSCF}_{ij} = \frac{\mathrm{M}_{ij}}{\mathrm{N}_{ij}} W_{ij} \quad (1)$$

Atmos. Chem. Phys. Discuss., https://doi.org/10.5194/acp-2018-225
Manuscript under review for journal Atmos. Chem. Phys.
Discussion started: 25 April 2018

Atmospheric Chemistry and Physics Discussions

where N_{ij} is the total number of trajectory segment endpoints that fall in the *ij* cell and M_{ij} is the number of endpoints for the same cell with arrival times at the sampling site corresponding to the pollutant concentrations higher than an arbitrary criterion value. In this study, the average concentration for each trace element was set as the criteria value. To suppress the erroneous and uncertainly of the small value of n_{ij}, the weighting function of W_{ij} reduced the PSCF values when the total number of the endpoints in a particular cell n_{ij} was less by approximately 3 times than the average N_{Ave} value of the endpoints per each cell (Han et al., 2005):

$$W_{ij} = \begin{cases} 1.00 & N_{ij} > 3N_{Ave} \\ 0.70 & 1.5N_{Ave} < N_{ij} \le 3N_{Ave} \\ 0.42 & N_{Ave} < N_{ij} \le 1.5N_{Ave} \\ 0.17 & 0 < N_{ij} \le N_{Ave} \end{cases} \quad (2)$$

3 Results and discussion

3.1 Classification of the typical pollution episodes

The air pollution during the cruise was classified into eight distinct episodes based on sampling locations, backward trajectory and photochemical aging processes (the T/B value) (Figure 1, Figure S1 and Table 1). The detailed meteorological information along YRC was also summarized in supplements. As shown in Figure S1, the first episode (EP1), staring from 22 to 23 November, was characterized as the sampled air masses from East China Sea, which brought the local industry and Shanghai harbor pollution. The ratio of T/B ranged from 1 to 2 with an average of 1.3 suggesting fresh air masses mixed by the aged ones. Air masses in the secondary episode (EP2), with B/T<1, originated from Anhui and Henan rural areas, carrying agriculture emission. Sampled air masses stagnated around Jiujiang to Wuhan from the third episode (EP3) to the fifth episode (EP5). However, the fourth episode (EP4) (near Wuhan) with the low average T/B ratio of 0.97 experienced a serious photochemical aging. Besides, the local air in EP4 was under low pressure system with high RH coupled with the low wind speeds that didn't favor the diffusion of the local pollutants (Figure S2). Both EP3 and EP5 (nearly Jiujiang) were characterized by high T/B value of 2.1, suggesting that these two pollution episodes were

contributed mainly by local fresh emissions. In the sixth episode (EP6), the wind direction shifted from southwest to northwest, and the vessel was traveling in the rural area of middle reach of Yangtze River, suggesting that air masses may originate from agricultural activities. Then, a cold front arrived and wind speed increased from average 3.84 m/s to 5.38 m/s (Table 2) with air masses transported from northern inland in the seventh episode (EP7), which were further supported by wind field (Figure S2) and a sharply RH decrease. The last episode (EP8) lied in the YRD region where highly intensive anthropogenic activities released a large amount of the pollutants. Air masses in EP8, with the average T/B value of 1.73, were expected to mixture of aged masses sources with local fresh emission. Overall, EP1 and EP8 (the YRD region) were mainly influenced by fresh local emission mixed by aged air masses, while agriculture emissions contributed mainly to EP2 and EP6. Both EP3 and EP5 were characterized by industries emission although the megapolis was not available in this region. The cruise stared on November 22, but the offline $PM_{2.5}$ samples were taken after November 25. The EP1 description was thus ignored in the present study.

3.2 Trace gases and fine particles measurements during YRC

3.2.1 The pollutants measured in the vessel

The off-line of $PM_{2.5}$ and $PM_{1.0}$ were sampled from 25 November to 5 December. Their detail information was also summarized in Table 1. The average mass concentration of $PM_{1.0}$ and $PM_{2.5}$ during YRC were 96.69 ± 22.18 μg m^{-3} and 119.29 ± 33.67 μg m^{-3}, respectively. The average ratio of $PM_{1.0}/PM_{2.5}$ was 0.8 ± 0.085, implying that $PM_{2.5}$ was mainly dominated by fine particles with the size of < 1 μm. The detailed meteorological information, including temperature (T), RH, pressure and wind speed (WS), and trace gases for pollution episodes were also summarized in Table 2. The peak $PM_{2.5}$ concentrations were observed in EP4 and EP7. However, there were obvious differences between EP4 and EP7 in the meteorological parameters and trace gases levels, indicating that these two pollution events were completely different. As mentioned in 3.1, air masses in EP4 were mainly originated from local emission, whereas EP7 was influenced by a long-transport of the pollutants.

As shown in Table 2, the average concentrations of CO, SO_2 and NO_X varied dramatically in the pollution episodes, mainly owing to local emissions, photochemical processes and meteorology conditions (Xu et al., 2011). Average concentrations of CO and SO_2 (993.96 ± 387.34 and 9.32 ± 4.33 ppbv, respectively) were slightly lower than those in cities in winter, including Wuhan (1024.00 and 13.30 ppbv) (Wang et al., 2017), Nanjing (1096.00 and 13.09 ppbv) (Sun et al., 2017), Chengdu (1440.00 and 12.60 ppbv) (Liao et al., 2017) and Shanghai (1067.20 and 18.90 ppbv) (Huang et al., 2012a). The CO level increased during the sampling and peaked in EP6 and EP7. Meanwhile, the SO_2 and NO_X levels were much lower in these two episodes, which was identified as the BB events. The mean CO concentration in EP7 was substantially enhanced and reached to 1224.88 ppbv, which was close to the level recorded at Shanghai during the harvest season of wheat (June) (Huang et al., 2012a). As reported previously, CO was the major gaseous pollutants released from BB (Huang et al., 2012a;Ding et al., 2013b). The SO_2 concentrations in EP3 and EP8 greatly increased, which were close to the SO_2 level in the haze event in Shanghai (Huang et al., 2012a). This was partly caused by local fresh emission (high T/B in EP3 and EP8). Besides EP6 and EP7 (BB), the NO_X concentration almost exceeded 50 ppbv along this cruise. The NO_X concentration peaked in EP3, which was identified as local emission region. Mean NO_x mass concentration in this cruise is 63.74 ± 41.08 ppbv, which was much higher than the mean levels in Shanghai (42.40ppbv, 2012) (Han et al., 2015) and Guangzhou (39.14ppbv, 2012) (Zou et al., 2015) that represented typical urban NO_X level. The high NO_X distribution along YRC revealed strong local emission from both edge of the Yangtze River. It could be supposed that lots of the pollution sources distributed on both the bank of the Yangtze River.

3.2.2 Regional distributions of the air pollutants by remote sense

The YRC region is one of the most polluted areas in China and the spatial distribution of various pollutants were regionally different. As shown in Figure 2a, high average values of AOD retrieved from MODIS MOD04 were observed in eastern Jiangsu and Shanghai, etc, where human and industries activities were concentrated, suggesting that anthropogenic emission was dominated. However, there was much missing data of AOD in central China due to heavy

clouds. As evidenced in Figure S3 by the MODIS true-color imagery on 28 November, thick clouds covered across central China. Besides, the average of AOD was about 0.45, which was slight lower than that in Shanghai in winter (0.55) (He et al., 2012) and background (0.65) in the North China plain. Besides, the AOD value in Northern China was higher than that in Southern China. As plotted in Figure 2b, CO surface mixing ratio calculated by MOPITT revealed that Shandong, Henan and Anhui were exposed to high CO column concentration. CO is an important tracer for the incomplete combustion sources, such as BB and fossil fuel combustions (Girach et al., 2014). BB should be the major source for CO in the grain-producing areas (Huang et al., 2012; Ding et al., 2013). As mentioned above, the peak CO level was also observed in Anhui (EP6 and EP7). The high levels of SO_2 were mainly observed in Anhui and stretched to the Shanghai area (Figure 2c). Whereas, the SO_2 level in the Wuhan and Nanjing urban areas were measured at the background pollution level. In general, NO_2 was regarded as a tracer for the local emission sources due to short lifetime in the atmosphere (Geng et al., 2009;Xu et al., 2011). NOx were significantly originated from vehicle and power plant emissions (Fu et al., 2013). One can see that the NO_2 emission was characterized by strong local source in north China and the YRD urban area, which are in good agreement with the previous reports (Lin, 2011;Zhao et al., 2013a).

3.3 The ionic composition and levoglucosan in $PM_{2.5}$ collected along the YRC

3.3.1 General characterization

The water-soluble ions constitute one of the dominant components in atmospheric aerosol and determine the aerosol acidity (Kerminen et al., 2001), accounting for 37.43% and 40.15% in $PM_{2.5}$ and $PM_{1.0}$, respectively. For the ionic concentration, the most abundant species hosted by $PM_{2.5}$ were SO_4^{2-} with an mean of 15.21 ± 6.69 μg m^{-3}, followed by NO_3^- (13.76 ± 4.99 μg m^{-3}), NH_4^+ (9.38 ± 4.35 μg m^{-3}), Ca^{2+} (2.23 ± 1.24 μg m^{-3}), Cl^- (1.94 ± 0.92 μg m^{-3}), Na^+ (1.29 ± 0.48 μg m^{-3}), K^+ (0.63 ± 0.22 μg m^{-3}) and Mg^{2+} (0.22 ± 0.07 μg m^{-3}) (Figure S4a). The mass concentration of SNA accounted for 85.89% of the total water-soluble ions in $PM_{2.5}$. Comparing with the previous reports (Figure 3), the SNA concentrations were lower than those collected

in the polluted cities in winter, including Beijing (38.90, 22.70 and 22.4 μg m^{-3}, respectively) (Wang et al., 2015a), Xi'an (39.7, 21.43 and 12.50 μg m^{-3}, respectively) (Xu et al., 2016a), Wuhan (29.80, 29.80 and 16.80 μg m^{-3}, respectively) (Zhang et al., 2015) and Chengdu (31.80, 15.5 and 15.5 μg m^{-3}, respectively) (Tao et al., 2014a). However, the concentration of SNA were higher than those collected in marine boundary layer, such as East China sea (29.80, 29.80 and 16.80 μg m^{-3}, respectively) (Nakamura et al., 2005), Northern South China Sea (7.80, 0.24 and 2.1 μg m^{-3}, respectively) (Zhang et al., 2007), South China sea (7.99, 0.08 and 1.083 μg m^{-3}, respectively) (Hsu et al., 2007), Taiwan Strait (5.20, 3.13and 1.50 μg m^{-3}, respectively) (Li et al., 2016), and Tuoji island in Bohai Rim (8.90, 5.80 and 1.40 μg m^{-3}, respectively) (Zhang et al., 2014). The SNA levels in the YRC was close to Shanghai in winter (11.7, 13.33 and 8.11 μg m^{-3}, respectively) (Zhou et al., 2016). The mass ratio of NO_3^-/SO_4^{2-} was regarded as a marker to distinguish mobile source vs. stationary source (Huang et al., 2013). The ratio of NO_3^-/SO_4^{2-} in this campaign was also close to Shanghai and lower than those in other cities, indicating that the mobile sources (traffic) contributed mainly to fine particles. Besides, the mass concentration of SO_4^{2-} definitely exceed the NO_3^- level in the marine boundary layer (Figure 3), indicating that marine was another important source for SO_4^{2-} (Calhoun et al., 1991). The average concentration of Ca^{2+}(2.23 μg m^{-3}) in this cruise was highest among all locations and cruises as summarized in Figure 3, followed Chengdu (2.10 μg m^{-3}), Wuhan (1.90 μg m^{-3}) and Xi'an (1.33 μg m^{-3}). As shown in Figure 3, Ca^{2+} also presented the higher concentration in the cities and decreased from inland to coastal of ocean, indicating that Ca^{2+} was mainly from terrace crustal (Xiao et al., 2017). However, the concentration of K^+ and Mg^{2+} in YRC were lower than most samples among all location (Figure 3). K^+ may originate from BB, sea salt and crustal dust. High average Ca^{2+} concentration in this campaign suggested that K^+ may come from crustal dust. Average Cl^- concentration was also lower than those in most cities (Figure 3). However, Na^+ was higher than the most reported values (Figure 4). Besides, the ratio of Cl^-/Na^+ among all location (Figure 3) were much higher than 1.17 (ratio of seawater), suggesting that anthropogenic sources, including BB and coal combustion, contributed the excessive Cl^- in

China cities (Li et al., 2015a;Zhang et al., 2013). The concentration of levoglucosan, a BB tracer, ranged from 0.015-0.18 μg m^{-3} with a mean value of 0.075 ± 0.047 μg m^{-3}, much higher than the average concentration of 0.0394 μg m^{-3} in Lin'an (30.3°N, 119.73°E) (a rural site of the YRD regions) (Liang et al., 2017), indicating that BB was also an major contributor to $PM_{2.5}$.

3.3.2 Distribution of the soluble ions and levoglucosan along the cruise

The concentrations and mass fractions of the major ions and levoglucosan in $PM_{2.5}$ are shown in Figure 4. The mass concentration of SNA with an average of 38.35 ± 15.17 μg/m^3 increased from coast to inland and exhibited the highest level (#6, 79.06 μg/m^3) in the Wuhan region (EP4), accounting for nearly 50% of local $PM_{2.5}$ mass. As mentioned above, SO_2 and NO_x also present the high concentration in this region. Furthermore, Wuhan and the surrounding regions were controlled by the low-pressure system with low WS and high RH (Figure S2), of which have been verified to cause haze episode (Zhao et al., 2013d;Quan et al., 2011;Wang et al., 2010). Besides, the mass fraction of SNA in $PM_{2.5}$ also peaked in rural region (EP2 and EP6), which was in accord with low ratio of T/B in these regions, suggesting that aerosol particles in rural region were well aged. Furthermore, the peak Cl^- concentration and its mass fraction in $PM_{2.5}$ also observed in Wuhan region. Thus, it's concluded that Wuhan and the surrounding regions suffered serious pollution with high SNA loading during sampling. In addition, the ratio of NO_3^-/SO_4^{2-} in the Wuhan area was close to the values of cities in Northern China (relatively low) (Figure 3), suggesting that the stationary source (such as: coal fired power station or stove emission) dominated in this area. The highest Cl^- concentration in this region also supported this result.

Contrary to SNA distribution (Figure 3), the concentration of Ca^{2+} along this cruise increased from mainland to costal of East China Sea and the peak Ca^{2+} mass fraction in $PM_{2.5}$ was measured in EP7 and EP8, probably due to its local floating dust. The highest concentration of 4.89 μg m^{-3} was observed on 3 December when the vessel was traveling through Nanjing. In the meanwhile, dust episode was verified by MODIS true-color image on 2 and 3 December (Figure S3), supported by a drastically decrease of RH with the prevailing northern wind (Table

353 2). Resembling Ca^{2+} distribution pattern, the maximal concentrations of Na^+ and K^+ in $PM_{2.5}$
354 were also measured during EP7. In general, it was well known that dust particles with high
355 alkalinity could firstly neutralize SO_4^{2-} and NO_3^- in aerosol particles, then atmospheric ammonia
356 was absorbed. The concentrations and mass fractions of SNA in $PM_{2.5}$ slightly increased at the
357 end of the cruise since carbonate in aerosol could enhance the uptake of acidic gases on particles
358 (Huang et al., 2010). In the meanwhile, the increasing mass ratio of NO_3^-/SO_4^{2-} in EP7 and EP8
359 was attributed to two main reasons. The mobile sources (such as: vehicle emission) increased
360 and released huge amount of NO_x when the vessel was close to the megacity (Huang et al.,
361 2013). Furthermore, NO_2 could transform into NO_3^- via the heterogeneous process on dust
362 aerosol surface (Nie et al., 2012).

363 The distribution of levogluscan is irregular parabolic from inland to coastal of sea. The
364 maximal value of levogluscan (0.18 μg m^{-3}) was observed in Anhui rural area (EP6), while the
365 levogluscan level in YRD region (EP8) was much lower. However, fire points couldn't be
366 observed apparently in the satellite-detected fire maps (http://firefly.geog.umd.edu/firemap/),
367 due to heavy cloud cover on 27 November and 1 December. During the whole campaign, it was
368 only collected one sample (#12, Figure S5) for BB which was verified by MODIS fire points,
369 due to a cold current blowing heavy clouds away (Figure S3). A slightly higher levoglucosan
370 concentration was observed in night that was attributed to the lower boundary layer at night and
371 BB for heating and cooking in the rural regions.

372 Ion balance gained by the major anions (SO_4^{2-}, NO_3^- and Cl^-) and cations (Na^+, NH_4^+, K^+, Ca^{2+},
373 Mg^{2+}) was furthermore calculated in this study. Both cation and anion are in the units of
374 equivalent concentration (μ eq m^{-3}). The linear correlation coefficient of cation *vs* anion for
375 $PM_{2.5}$ and $PM_{1.0}$ were 0.828 and 0.837 (Figure S6a), respectively, implying that the major ions
376 in $PM_{2.5}$ and $PM_{1.0}$ could be contributed by same sources. There is a good correlation ($R^2 > 0.93$)
377 between NH_4^+ (equivalent concentration) and the sum of SO_4^{2-} and NO_3^- (equivalent
378 concentration) in $PM_{2.5}$, which suggested a good quality of data. Additionally, the relationship
379 between NH_4^+ and Ca^{2+} versus SO_4^{2-} and NO_3^- was also investigated. As plotted in Figure S6b,

the slopes of linear regression lines for $[NH_4^+ + Ca^{2+}]$ *vs* $[SO_4^{2-} + NO_3^-]$ in $PM_{2.5}$ and $PM_{1.0}$ were 1.171 and 1.154, respectively, suggesting that the alkaline substance in aerosol could neutralize SO_4^{2-} and NO_3^- completely during YRC.

3.4 Elemental concentration, spatial distribution and sources identification

3.4.1 General characterization

A total of 17 elements in the $PM_{1.0}$ and $PM_{2.5}$ samples collected during YRC were measured, and their average concentrations are summarized in Table 3. For comparison, the data reported previously in the megacities (in winter) and the cruises are also outlined in Table 4. Ca showed the highest concentration among all elements (Table 3) at all locations (Table 4), and shared 2.16% on average in $PM_{2.5}$, partly due to a cold front with floating dust in this campaign. The secondary highest concentration among all elements was Fe (Table 3). This concentration (1.64 μg m^{-3}) in the campaign were higher than those at many urban sites, such as Beijing (1.55 μg m^{-3}) (Zhao et al., 2013c), Shanghai (0.56 μg m^{-3}) (Huang et al., 2012b) and Guangzhou (0.16 μg m^{-3}) (Lai et al., 2016), probably due to numerous steel industries/shipyard distributed on both two banks of the Yangtze River. Other elements decreased from K (865.88 ng m^{-3}) to Tl (0.32 ng m^{-3}). Pb and Zn contributed the high levels for heavy metals in $PM_{2.5}$. In addition to inland cities, such as Beijing (Zhao et al., 2013c), Wuhan (Zhang et al., 2015) and Chengdu (Tao et al., 2014a), average concentration of Pb and Zn along the YRC was much higher than those in the other regions and cruises (Table 4). Both Pb and Zn could originate from coal combustion or mineral industry, which were related to energy structure and industrial layout in MLYP (Zhao et al., 2013c;Huang et al., 2013;Zhang et al., 2015;Tao et al., 2014a;Lai et al., 2016;Li et al., 2016;Zhao et al., 2015).

The enrichment factor (EF) was applied to identify the trace elements from crustal or anthropogenic sources. The formula to evaluate EF was:

$$EF_i = (X_i/X_R)_{aerosol} / (X'_i/X'_R)_{crust} \quad (3)$$

of which EF_i is the enrichment factor of element *i*; X_i and X_R are the concentrations of element *i* and reference element of R in aerosol, respectively; X'_i and X'_R are the background content

of elements in the MLYP soil (Wei et al., 1991). Al was considered to be originated from soil, thus it was selected as the reference element for calculation. Trace elements with EF < 10 included: Al, Co, K, Mg, and Na, all of which were regarded from crustal or re-suspension of the local soil. The species with higher 10 < EFs < 100 were thought to be the mixture of the crustal and anthropogenic sources, including Cr, Cu, Ni and V. The elements with EF > 100, including Ca, Zn, Se, Pb, As, Mo, Fe, and Cd, were attributed to be originated from anthropogenic activities.

3.4.2 Source apportionments and regional distribution of the main elements in $PM_{2.5}$

In order to identify the source of contaminated elements and their geographical distribution, PCA was applied to classify the main source of trace elements in $PM_{2.5}$ using the rotate component matrix and PSCF for individual elements was performed to estimate the potential sources.

As shown in Figure 5a, trace elements were classified into four categories (PCA), which could explain 86.73% of the variance. The first component (component 1) could account for 38.48% of the variance, which was considered to be originated from coal burning, including high loadings of Cd, As, Pb, Tl and Se. Particularly, Se was generally considered as a tracer for coal combustion due to production under high temperature environment. It was well known that Se hosted by fine particles after the rapid gas-to-particle conversion could undergo a long-range transport (Nriagu, 1989;Wen and Carignan, 2007). A significant correlation (R^2 = 0.71) between SO_4^{2-} and Se are shown in Figure S4b. Furthermore, As and Pb mainly originated from coal burning after phasing out of leaded gasoline in China since 1997 (Xu et al., 2012), both of which showed the high correlations with Se. Meanwhile, component 1 showed the high concentration in EP4 and EP5 (Figure 5b) when the ship anchored in Wuhan and travelled through Jiujiang. As illustrated in Figure 6a-d, As, Cd, Pb and Se showed the similar source region distributions. The higher PSCF values in Hubei, Hunan and Jiangxi provinces coincided well with the uneven regional distribution of the residential coal consumption (Figure S7) in central China, suggesting coal-related PM pollution was quite serious in this region during the cruise.

435 The secondary component (component 2) with a variation of 25.45%, contributed by high
436 loading of Al, Mg, Ca, and K, all of which obviously represented the crustal or soil materials
437 and showed the low EF values (EFs< 10, except Ca). The high concentration spike of crustal
438 elements occurred in EP7 (Figure 5b). A sharp decrease of RH (Table 2) indicated that a cold
439 front arrived, accompanying by floating dust. As shown in Figure 6e-h, the YRD region and
440 the Loess Plateau with highest PSCF values were identified as important source regions and
441 pathways for crustal elements of Al, K, Mg and Ca. Meanwhile, the central China also showed
442 the distribution of K and Mg, for which the coal combustion in this region could be primary
443 responsible. Furthermore, Ca showed the high EFs (EFs > 100), suggesting that the crustal
444 material may not derive from natural sources, but from anthropogenic re-suspension of road or
445 construction activities along of the Yangtze River. To further evaluate the impact of
446 anthropogenic Ca, the equation below was applied:

447 $$Ca_{anthropogenic} = Ca_{total} - Al_{total} \times (Ca/Al)_{crust} \quad (4)$$

448 $(Ca/Al)_{crust}$ is ratio of Ca to Al in crust and its value is 0.5. According to this method, the
449 average $Ca_{anthropogenic}$ concentration was 2.15 μg m^{-3} and the peak level reached to 3.42 μg m^{-3}
450 on December 3. IF all of $Ca_{anthropogenic}$ in the samples of other cities and cruises (Table 4) were
451 calculated by this method, its level in this cruise was much higher than those in other samples,
452 suggesting that anthropogenic dust was dominated and distributed in the YRD region during
453 the period.

454 Component 3, accounting for 15.14% of variation, was considered to be the primary of V,
455 Co and Ni. Both V and Ni was often used to be a tracer of heavy oil combustion (Zhao et al.,
456 2013b;Becagli et al., 2017). The high concentrations of V and Ni were observed when the ship
457 was anchored at the Waigaoqiao port of Shanghai (EP8) (Figure 5b), where some field
458 observations have identified that heavy oil combustion exert a significant impact on the local
459 air quality (Zhao et al., 2013b;Fu et al., 2014;Ding et al., 2017;Liu et al., 2017). It was also
460 reported that the combustion of heavy oil emitted smaller particles with the size of < 0.1μm and
461 the transition metals of Ni and V were greatly enriched (Jang et al., 2007). Ni hosted in fine

462 particles (Figure 6i) had almost same spatial distribution with Cr and the YDR, Jiangsu, east of
463 Anhui, and the Mongolian plateau were identified as the major source regions and pathways.
464 However, the high PSCF values for fine particle V (Figure 6j) were only derived from the YDR
465 and Mongolian plateau, that's possible reason that V was considered origination from heavy oil
466 combustion while Ni have other sources (Table S1) (Zhao et al., 2013b).

467 The fourth component (component 4) showed high loadings of Mn, Co, Zn and Fe, all of
468 which could explain 7.33% of the variance. Fe exhibited the high EFs value, indicating that
469 they may originate from anthropogenic activities. Anthropogenic Fe was usually considered to
470 be originated from steel factory and/or shipyard, both of which were widely distributed over
471 the YRC region (Fu et al., 2014). The temporal variations of component 4 peaked nearly in
472 Wuhan and Shanghai (EP4, EP7 and EP8) (Figure 5b) where China Baowu steel industry and
473 numerous shipyards were located in this region (Ivošević et al., 2016). Fe, Co, Mn and Zn in
474 fine particles displayed similar regional distributions (Figure 6l-o). The significantly high PSCF
475 values in the YRD region were attributed to the intensive distribution of steel industries in East
476 of Anhui, Jiangsu and Shanghai and shipyards on the banks of the Yangtze River. However,
477 the high PSCF value of Zn also exhibited high value in Hubei, Henan and Shanxi (Figure 6l),
478 probably due to the influence of coal combustion and nonferrous metal smelting activities in
479 these regions (Li et al., 2015b). Overall, it should be noted that regional anthropogenic sources
480 were dominant origins of trace elements in fine particles collected along this cruise.

481 **3.5 Ship emission**

482 **3.5.1 Primary of ship emission**

483 Over the past few decades, China's rapid economic development leads to huge cargo transports
484 by ship in the Yangtze River channel. However, there is lack of data for ship emission along the
485 Yangtze River channel, especially in the inland area. It was well known that the ratio of V to
486 Ni was used to judge whether ship emission could influence air quality (Isakson et al., 2001).
487 The average ratio of V/Ni over the present cruise is 1.27, which was in good agreement with
488 the previous studies (Pandolfi et al., 2011;Zhang et al., 2014). Although ratio of V/Ni was used
489 to judge whether ship emission could influence air quality, it was still a challenge to distinguish

V from refineries and ship plume. So, high-resolution back-trajectories and high-resolution of the ship position from the AIS data were applied to identify ship plume during this cruise (Figure S8). As plotted in Figure 7, the number of ship from AIS were closely related to the V concentration. From the inland to the coastal of East China Sea, the V concentration hosted by fine particles generally increased and reached the highest level of 0.06 μg m^{-3} on 4 December when the vessel berthed in the anchorage of the Yangtze River estuary. Meanwhile, air masses in this evening originated from the port and anchorage (Figure S8). Hence, the V in the fine particles could be possibly attributed by the ship engine emission in Shanghai port..

The contribution of primary ship emission to $PM_{2.5}$ could be calculated by the equation developed by (Agrawal et al. (2009):

$$PM_a = < r > \times V_a / < F_{V,HFO} > \quad (5)$$

where PM_a represents the primary $PM_{2.5}$ concentration estimated (μg m^{-3}); $< r >$ is average ratio of $PM_{2.5}$ to normalized V emitted (ppm); V_a represents the V amount of the samples (μg m^{-3}) during YRC and is the V content of heavy oil on average from the vessels (ppm). The value of $< r >$ was set as 8205.8 ppm according to Agrawal et al. (2009) report. The value of $< F_{V,HFO} >$ was set as 65.3 ppm, of which represents of the average V content (Zhao et al., 2013b). The average concentration of the primary ship emission was 1.19 μg m^{-3}, ranging from 0.02 to 7.37 μg m^{-3}. The peak level of the estimated primary ship emission was observed in Shanghai harbor.

3.5.2 SO_4^{2-}, NO_3^- and OC emitted from ships

To further explore the contribution of the ship plume to secondary fine particles, a lower limit of the SO_4^{2-}/V, NO_3^-/V, EC/V and OC/V ratios (equal to the average minus one standard deviation) was applied to estimate the particulate from heavy oil combustion in the Yangtze River channel (Becagli et al., 2017). As presented in Figure S9a-b, the mass ratio of SO_4^{2-}/V and NO_3^-/V decreased rapidly with increasing V concentration. According to ship traffic numbers, weather condition and the component of heavy diesel oil combustion emissions, the samples

516 with V > 15 ng m^{-3} were mainly considered as the ship emission. Hence, SO_4^{2-}, NO_3^-, EC and
517 OC in the samples with V > 15 ng m^{-3} were assumed to be from ship plume.
518 The limit ratio of SO_4^{2-} /V, NO_3^- /V and OC/V, and the estimation of the ship plume
519 contributions to SO_4^{2-}, NO_3^-, OC and $PM_{2.5}$ are summarized in Table S2 in supplements. The
520 minimum ratio of NO_3^-/V in this campaign was nearly twice larger than the limit ratio for SO_4^{2-}
521 /V, which was contrary to the previous report with higher SO_4^{2-} observed in summer on the island
522 of Lampedusa (35.5°N, 12.6°E) in the central Mediterranean. In general, SO_4^{2-} and NO_3^- in
523 aerosol were formed from gas precursors of SO_2 and NO_X, respectively, both of which were
524 complete different for lift-time and chemical processes in the atmosphere. High T and RH could
525 accelerate the chemical process of SO_2 to SO_4^{2-} (Zhou et al., 2016). However, NO_3^- was in gas-
526 aerosol equilibrium with gaseous HNO_3. So, low T and RH were conducive to NO_3^- formation
527 in aerosol (Matthias et al., 2010;Wang et al., 2016). One reason for this discrepancy was
528 probably meteorological and photochemical conditions, which may be attributed to low sulfur
529 conversion rates and particulate NO_3^- dominated in low temperature and moisture in winter in
530 this cruise (Table 2). On the other hand, NO_3^- may have other sources in our samples (Shanghai),
531 whereas Lampedusa was a remote site (Becagli et al., 2017). The average estimated
532 concentration of minimum SO_4^{2-} derived from ship emission was 1.38 μg m^{-3} during YRC,
533 which was similar to the value measured in the Mediterranean (Becagli et al., 2017;Becagli,
534 2012).
535 EC and OC were also estimated by the same methods for SO_4^{2-} and NO_3^- for calculation the
536 lower limit for OC/V and EC/V ratio in the ship plume (Figure S9c-d). Besides, the correlation
537 of V with EC (R^2 = 0.71) have high value, suggesting that V and EC have same
538 sources(Agrawal et al., 2009). In this cruise, the total OC were estimated from OC measured
539 through a conversion factor of 1.8, due to typically fresh emission and weak light in winter
540 (Becagli et al., 2017). The total average of ship traffic in $PM_{2.5}$ was 8.46 μg m^{-3}, nearly
541 occupying 7.73% of total $PM_{2.5}$ during YRC. However, ship plume could reach to 52.28% of
542 total $PM_{2.5}$ when the vessel berthed in that Shanghai harbor. It is noted that the ship engine

emission decreased from Shanghai port to inland area. One reason for this was correspond to the density of ship in the Yangtze River channel. On the other hand, fuel oils were completely different between the ship travelling in inland waterway and the oceangoing vessel. In general, ship inland waterway run on mainly light diesel which contain low heavy metals (such as: V, Ni) comparing with marine heavy oil (Table S1). So, it is urgent to establish emission control area (ECA) in Shanghai ports.

4 Conclusions. In order to better characterize air pollution over the region of MLYP, an intensive atmospheric observation was conducted during YRC. A combine of ship-suit measurements of trace gases and aerosol samples for fine particles were used to characterize the air pollution in this region. The average concentrations of $PM_{1.0}$ and $PM_{2.5}$ were 96.69 ± 22.18 μg m^{-3} and 119.29 ± 33.67 μg m^{-3} during the cruise, respectively. The most abundant species in $PM_{2.5}$ were SO_4^{2-} with the average concentration of 15.21 ± 6.69 μg/m^3, followed by NO_3^- (13.76 ± 4.99μg/m^3), NH_4^+ (9.38 ± 4.35μg/m^3), Ca^{2+} (2.23 ± 1.24μg/m^3), respectively. Combined with satellite data, back trajectory, principle component analysis (PCA), and potential source contribution functions (PSCF), chemical composition in $PM_{2.5}$ manifested greatly geographical difference and diverse anthropogenic emission sources. Wuhan undertook SNA (including SO_4^{2-}, NO_3^- and NH_4^+), accounting for nearly 50% of $PM_{2.5}$. The significant correlation between Se and SO_4^{2-} corroborated that coal combustion may play a key role on the SNA formation. The concentration of levoglucosan in $PM_{2.5}$ and CO column level from the satellite data were greatly enhanced in the rural area (Anhui and Jiangxi), indicating that BB from the both shores of the Yangtze river may make remarkable contribution to rural area. Furthermore, the crustal elements of Al and Ca presented high levels in the YRD regions and the relative high enrichment factors (EFs) of Ca (EFs > 100) coupling with the PSCF analysis suggested the crustal material may derive from re-suspension of dust from road and construction activity along the banks of the Yangtze river. Ship engine emission displayed a significant effect on the air quality and could contribute to more than 50% of the total $PM_{2.5}$ in the Shanghai ports. As far as we know, this is the first comprehensive measurement of air

quality over the MLYP region using a vessel mobile platform. The data shown herein suggested that the differentiated control measures in accordance with local pollution characterizations should be applied to tackle air pollution.

ACKNOWLEDGMENTS

This work was supported by the Ministry of Science and Technology of China (No. 2016YFC0202700, 2014BAC22B00), the National Natural Science Foundation of China (No. 91743202, 21527814) and Marie Skłodowska-Curie Actions (690958-MARSU-RISE-2015).

578 **References:**

579 Ackerman, A. S., Kirkpatrick, M. P., Stevens, D. E., and Toon, O. B.: The impact of humidity
580 above stratiform clouds on indirect aerosol climate forcing, Nature, 432, 1014, 2004.
581 Agrawal, H., Eden, R., Zhang, X., Fine, P. M., Katzenstein, A., Miller, J. W., Ospital, J., and
582 Teffera, S.: Primary particulate matter from ocean-going engines in the Southern California Air
583 Basin, Environ. Sci. Technol., 43, 5398-5402, 2009.
584 An, J., Wang, H., Shen, L., Zhu, B., Zou, J., Gao, J., and Kang, H.: Characteristics of new
585 particle formation events in Nanjing, China: Effect of water-soluble ions, Atmos. Environ., 108,
586 32-40,doi: 10.1016/j.atmosenv.2015.01.038, 2015.
587 Baltrenas, P., Baltrenaite, E., Sereviciene, V., and Pereira, P.: Atmospheric BTEX
588 concentrations in the vicinity of the crude oil refinery of the Baltic region, Environ. Monit.
589 Assess., 182, 115-127, 2011.
590 Becagli, S., Anello, F., Bommarito, C., Cassola, F., Calzolai, G., Di Iorio, T., di Sarra, A.,
591 Gómez-Amo, J.-L., Lucarelli, F., Marconi, M., Meloni, D., Monteleone, F., Nava, S., Pace, G.,
592 Severi, M., Sferlazzo, D. M., Traversi, R., and Udisti, R.: Constraining the ship contribution to
593 the aerosol of the central Mediterranean, Atmos. Chem. Phys., 17, 2067-2084,doi: 10.5194/acp-
594 17-2067-2017, 2017.
595 Becagli, S. S., D. M.Pace, G.di Sarra, A.Bommarito, C.Calzolai, G.Ghedini, C.Lucarelli,
596 F.Meloni, D.Monteleone, F.Severi, M.Traversi, R.Udisti, R.: Evidence for heavy fuel oil
597 combustion aerosols from chemical analyses at the island of Lampedusa: a possible large role
598 of ships emissions in the Mediterranean, Atmos. Chem. Phys., 12, 3479-3492,doi: 10.5194/acp-
599 12-3479-2012, 2012.
600 Calhoun, J. A., Bates, T. S., and Charlson, R. J.: Sulfur isotope measurements of submicrometer
601 sulfate aerosol particles over the Pacific Ocean, Geophys. Res. Lett., 18, 1877-1880,doi:
602 10.1029/91gl02304, 1991.
603 Chameides, W. L., Yu, H., Liu, S. C., Bergin, M., Zhou, X., Mearns, L., Wang, G., Kiang, C.
604 S., Saylor, R. D., and Luo, C.: Case study of the effects of atmospheric aerosols and regional

haze on agriculture: an opportunity to enhance crop yields in China through emission controls?, Proc. Nat. Acad. Sci. U.S.A., 96, 13626-13633, 1999.

Cheng, Z., Wang, S., Fu, X., Watson, J. G., Jiang, J., Fu, Q., Chen, C., Xu, B., Yu, J., and Chow, J. C.: Impact of biomass burning on haze pollution in the Yangtze River delta, China: a case study in summer 2011, Atmos. Chem. Phys., 14, 4573-4585,doi: 10.5194/acp-14-4573-2014, 2014.

Coggon, M. M., Sorooshian, A., Wang, Z., Metcalf, A. R., Frossard, A. A., Lin, J. J., Craven, J. S., Nenes, A., Jonsson, H. H., Russell, L. M., Flagan, R. C., and Seinfeld, J. H.: Ship impacts on the marine atmosphere: insights into the contribution of shipping emissions to the properties of marine aerosol and clouds, Atmos. Chem. Phys., 12, 8439-8458,doi: 10.5194/acp-12-8439-2012, 2012.

Ding, A. J., Fu, C. B., Yang, X. Q., Sun, J. N., Petäjä, T., Kerminen, V. M., Wang, T., Xie, Y., Herrmann, E., and Zheng, L. F.: Intense atmospheric pollution modifies weather: a case of mixed biomass burning with fossil fuel combustion pollution in eastern China, Atmos. Chem. Phys., 13, 10545-10554,doi: 10.5194/acp-13-10545-2013, 2013a.

Ding, X., Wang, X., Xie, Z., Zhang, Z., and Sun, L.: Impacts of Siberian biomass burning on organic aerosols over the North Pacific Ocean and the Arctic: primary and secondary organic tracers, Environ. Sci. Technol., 47, 3149-3157, 2013b.

Ding, X., Kong, L., Du, C., Zhanzakova, A., Wang, L., Fu, H., Chen, J., Yang, X., and Cheng, T.: Long-range and regional transported size-resolved atmospheric aerosols during summertime in urban Shanghai, Sci. Total Environ., 583, 334-343, 2017.

Draxler, R. R., and Hess, G. D.: An overview of the HYSPLIT_4 modelling system for trajectories, Aust. Meteorol. Mag., 47, 295-308, 1998.

Fan, Q., Zhang, Y., Ma, W., Ma, H., Feng, J., Yu, Q., Yang, X., Ng, S. K., Fu, Q., and Chen, L.: Spatial and Seasonal Dynamics of Ship Emissions over the Yangtze River Delta and East China Sea and Their Potential Environmental Influence, Environ. Sci. Technol., 50, 1322-1329, 2016.

Fu, H. B., Shang, G. F., Lin, J., Hu, Y. J., Hu, Q. Q., Guo, L., Zhang, Y. C., and Chen, J. M.:

633 Fractional iron solubility of aerosol particles enhanced by biomass burning and ship emission
634 in Shanghai, East China, Sci. Tot. Environ., 481, 377-391, 2014.
635 Fu, X., Wang, S., Zhao, B., Xing, J., Cheng, Z., Liu, H., and Hao, J.: Emission inventory of
636 primary pollutants and chemical speciation in 2010 for the Yangtze River Delta region, China,
637 Atmos. Environ., 70, 39-50, 2013.
638 Gaston, C. J., Quinn, P. K., Bates, T. S., Gilman, J. B., Bon, D. M., Kuster, W. C., and Prather,
639 K. A.: The impact of shipping, agricultural, and urban emissions on single particle chemistry
640 observed aboard the R/V Atlantis during CalNex, J. Geophys. Res. Atmos., 118, 5003-5017,doi:
641 10.1002/jgrd.50427, 2013.
642 Geng, F., Zhang, Q., Tie, X., Huang, M., Ma, X., Deng, Z., Yu, Q., Quan, J., and Zhao, C.:
643 Aircraft measurements of O_3, NOx, CO, VOCs, and SO_2 in the Yangtze River Delta region,
644 Atmos. Environ., 43, 584-593, 2009.
645 Girach, I., Nair, V. S., Babu, S. S., and Nair, P. R.: Black carbon and carbon monoxide over
646 Bay of Bengal during W_ICARB: Source characteristics, Atmos. Environ., 94, 508-517, 2014.
647 Han, T., Qiao, L., Zhou, M., Qu, Y., Du, J., Liu, X., Lou, S., Chen, C., Wang, H., and Zhang,
648 F.: Chemical and optical properties of aerosols and their interrelationship in winter in the
649 megacity Shanghai of China, J. Environ. Sci., 27, 59-69, 2015.
650 Han, Y.-J., Holsen, T. M., Hopke, P. K., and Yi, S.-M.: Comparison between back-trajectory
651 based modeling and Lagrangian backward dispersion modeling for locating sources of reactive
652 gaseous mercury, Environ. Sci. Technol., 39, 1715-1723, 2005.
653 He, Q., Li, C., Geng, F., Yang, H., Li, P., Li, T., Liu, D., and Pei, Z.: Aerosol optical properties
654 retrieved from Sun photometer measurements over Shanghai, China, J. Geophys. Res. Atmos.,
655 117, D16204,doi: 10.1029/2011jd017220, 2012.
656 Hopke, P. K., Barrie, L. A., Li, S. M., Cheng, M. D., Li, C., and Xie, Y.: Possible sources and
657 preferred pathways for biogenic and non-sea-salt sulfur for the high Arctic, J. Geophys. Res.
658 Atmos., 100, 16595-16603,doi: 10.1029/95JD01712, 1995.
659 Hsu, S.-C., Liu, S. C., Kao, S.-J., Jeng, W.-L., Huang, Y.-T., Tseng, C.-M., Tsai, F., Tu, J.-Y.,
660 and Yang, Y.: Water-soluble species in the marine aerosol from the northern South China Sea:

661 High chloride depletion related to air pollution, J. Geophys. Res., 112,doi:
662 10.1029/2007jd008844, 2007.
663 Huang, K., Zhuang, G., Lin, Y., Fu, J. S., Wang, Q., Liu, T., Zhang, R., Jiang, Y., Deng, C.,
664 and Fu, Q.: Typical types and formation mechanisms of haze in an Eastern Asia megacity,
665 Shanghai, Atmos. Chem. Phys., 12, 105,doi: 10.5194/acp-12-105-2012, 2012a.
666 Huang, K., Zhuang, G., Lin, Y., Wang, Q., Fu, J. S., Zhang, R., Li, J., Deng, C., and Fu, Q.:
667 Impact of anthropogenic emission on air quality over a megacity–revealed from an intensive
668 atmospheric campaign during the Chinese Spring Festival, Atmos. Chem. Phys., 12, 11631-
669 11645,doi: 10.5194/acp-12-11631-2012, 2012b.
670 Huang, K., Zhuang, G., Lin, Y., Wang, Q., Fu, J. S., Fu, Q., Liu, T., and Deng, C.: How to
671 improve the air quality over megacities in China: pollution characterization and source analysis
672 in Shanghai before, during, and after the 2010 World Expo, Atmos. Chem. Phys., 13, 5927-
673 5942,doi: 10.5194/acp-13-5927-2013, 2013.
674 Isakson, J., Persson, T. A., and Lindgren, E. S.: Identification and assessment of ship emissions
675 and their effects in the harbour of Göteborg, Sweden, Atmos. Environ., 35, 3659-3666, 2001.
676 Ivošević, T., Stelcer, E., Orlić, I., Bogdanović Radović, I., and Cohen, D.: Characterization and
677 source apportionment of fine particulate sources at Rijeka, Croatia from 2013 to 2015, Nucl.
678 Instrum. Methods. Phys. Res. B., 371, 376-380, 2016.
679 Jalkanen, J., Johansson, L., and Kukkonen, J.: A comprehensive inventory of ship traffic
680 exhaust emissions in the European sea areas in 2011, Atmos. Chem. Phys., 16, 71-84, 2015.
681 Jang, H. N., Lee, S. J. H., Hwang, K. W., Yoo, J. I., Sok, C. H., and Kim, S. H.: Formation of
682 fine particles enriched by V and Ni from heavy oil combustion: Anthropogenic sources and
683 drop-tube furnace experiments, Atmos. Environ., 41, 1053-1063, 2007.
684 Jiang, T., Kundzewicz, Z. W., and Su, B.: Changes in monthly precipitation and flood hazard
685 in the Yangtze River Basin, China, Int. J. Climatol., 28, 1471-1481, 2008.
686 Jones, A. D. L. A., Roberts, D. L., and Slingo, A.: A climate model study of indirect radiative
687 forcing by anthropogenic sulphate aerosols, Nature, 370, 450-453, 1994.
688 Kang, H., Zhu, B., Su, J., Wang, H., Zhang, Q., and Wang, F.: Analysis of a long-lasting haze

episode in Nanjing, China, Atmos. Res., 120-121, 78-87, 2013a.

Kang, H., Zhu, B., Su, J., Wang, H., Zhang, Q., and Wang, F.: Analysis of a long-lasting haze episode in Nanjing, China, Atmos. Res., 78-87, 2013b.

Kerminen, V.-M., Hillamo, R., Teinilä, K., Pakkanen, T., Allegrini, I., and Sparapani, R.: Ion balances of size-resolved tropospheric aerosol samples: implications for the acidity and atmospheric processing of aerosols, Atmos. Environ., 35, 5255-5265, 2001.

Kong, S., Li, X., Li, L., Yin, Y., Chen, K., Yuan, L., Zhang, Y., Shan, Y., and Ji, Y.: Variation of polycyclic aromatic hydrocarbons in atmospheric $PM_{2.5}$ during winter haze period around 2014 Chinese Spring Festival at Nanjing: Insights of source changes, air mass direction and firework particle injection, Sci. Tot. Environ., 520, 59-72, 2015.

Lai, S., Zhao, Y., Ding, A., Zhang, Y., Song, T., Zheng, J., Ho, K. F., Lee, S.-c., and Zhong, L.: Characterization of $PM_{2.5}$ and the major chemical components during a 1-year campaign in rural Guangzhou, Southern China, Atmos. Res., 167, 208-215, 2016.

Li, C., Ma, Z., Chen, J., Wang, X., Ye, X., Wang, L., Yang, X., Kan, H., Donaldson, D. J., and Mellouki, A.: Evolution of biomass burning smoke particles in the dark, Atmos. Environ., 120, 244-252, 2015a.

Li, T.-C., Yuan, C.-S., Hung, C.-H., Lin, H.-Y., Huang, H.-C., and Lee, C.-L.: Chemical Characteristics of Marine Fine Aerosols over Sea and at Offshore Islands during Three Cruise Sampling Campaigns in the Taiwan Strait– Sea Salts and Anthropogenic Particles, Atmos. Chem. Phys. Discuss., 1-27,doi: 10.5194/acp-2016-384, 2016.

Li, T., Wang, Y., Li, W. J., Chen, J. M., Wang, T., and Wang, W. X.: Concentrations and solubility of trace elements in fine particles at a mountain site, southern China: regional sources and cloud processing, Atmos. Chem. Phys., 15, 8987-9002,doi: 10.5194/acp-15-8987-2015, 2015b.

Liang, L., Engling, G., Zhang, X., Sun, J., Zhang, Y., Xu, W., Liu, C., Zhang, G., Liu, X., and Ma, Q.: Chemical characteristics of $PM_{2.5}$ during summer at a background site of the Yangtze River Delta in China, Atmos. Res., 198, 163-172, 2017.

Liao, T., Wang, S., Ai, J., Gui, K., Duan, B., Zhao, Q., Zhang, X., Jiang, W., and Sun, Y.:

717 Heavy pollution episodes, transport pathways and potential sources of $PM_{2.5}$ during the winter
718 of 2013 in Chengdu (China), Sci. Total Environ., 584, 1056-1065, 2017.
719 Lin, J. T.: Satellite constraint for emissions of nitrogen oxides from anthropogenic, lightning
720 and soil sources over East China on a high-resolution grid, Atmos. Chem. Phys., 11, 29807-
721 29843,doi: 10.5194/acp-12-2881-2012, 2011.
722 Liu, J. P., Xu, K. H., Li, A. C., Milliman, J. D., Velozzi, D. M., Xiao, S. B., and Yang, Z. S.:
723 Flux and fate of Yangtze River sediment delivered to the East China Sea, Geomorphology, 85,
724 208-224, 2007.
725 Liu, Z., Lu, X., Feng, J., Fan, Q., Zhang, Y., and Yang, X.: Influence of Ship Emissions on
726 Urban Air Quality: A Comprehensive Study Using Highly Time-Resolved Online
727 Measurements and Numerical Simulation in Shanghai, Environ. Sci. Technol., 51, 202-211,
728 2017.
729 Matthias, V., Bewersdorff, I., Aulinger, A., and Quante, M.: The contribution of ship emissions
730 to air pollution in the North Sea regions, Environ. Pollut., 158, 2241-2250,doi:
731 10.1016/j.envpol.2010.02.013, 2010.
732 Moldanová, J., Fridell, E., Popovicheva, O., Demirdjian, B., Tishkova, V., Faccinetto, A., and
733 Focsa, C.: Characterisation of particulate matter and gaseous emissions from a large ship diesel
734 engine, Atmos. Environ., 43, 2632-2641, 2009.
735 Nakamura, T., Matsumoto, K., and Uematsu, M.: Chemical characteristics of aerosols
736 transported from Asia to the East China Sea: an evaluation of anthropogenic combined nitrogen
737 deposition in autumn, Atmos. Environ., 39, 1749-1758, 2005.
738 Novakov, T., and Penner, J. E.: Large contribution of organic aerosols to cloud-condensation-
739 nuclei concentrations, Nature, 365, 823-826, 1993.
740 Nriagu, J. O.: A global assessment of natural sources of atmospheric trace metals, Nature, 338,
741 47-49, 1989.
742 Pandis, S. N., Capaldo, K., Corbett, J. J., Kasibhatla, P., and Fischbeck, P.: Effects of ship
743 emissions on sulphur cycling and radiative climate forcing over the ocean, Nature, 400, 743-
744 746, 1999.

745 Pandolfi, M., Gonzalez-Castanedo, Y., Alastuey, A., Jd, D. L. R., Mantilla, E., As, D. L. C.,
746 Querol, X., Pey, J., Amato, F., and Moreno, T.: Source apportionment of PM_{10} and $PM_{2.5}$ at
747 multiple sites in the strait of Gibraltar by PMF: impact of shipping emissions, Environ Sci Pollut
748 Res, 18, 260-269, 2011.
749 Pöschl, U.: Atmospheric aerosols: composition, transformation, climate and health effects,
750 Angew. Chem. Int. Ed., 44, 7520-7540, 2005.
751 Quan, J., Zhang, Q., He, H., Liu, J., Huang, M., and Jin, H.: Analysis of the formation of fog
752 and haze in North China Plain (NCP), Atmos. Chem. Phys., 11, 8205-8214,doi: 10.5194/acp-
753 11-8205-2011, 2011.
754 Seaton, A., Godden, D., MacNee, W., and Donaldson, K.: Particulate air pollution and acute
755 health effects, The lancet, 345, 176-178, 1995.
756 Shen, G. F., Yuan, S. Y., Xie, Y. N., Xia, S. J., Li, L., Yao, Y. K., Qiao, Y. Z., Zhang, J., Zhao,
757 Q. Y., and Ding, A. J.: Ambient levels and temporal variations of $PM_{2.5}$ and PM_{10} at a residential
758 site in the mega-city, Nanjing, in the western Yangtze River Delta, China, Journal of
759 Environmental Science and Health, Part A, 49, 171-178, 2014.
760 Stier, P., Feichter, J., Kinne, S., Kloster, S., Vignati, E., Wilson, J., Ganzeveld, L., Tegen, I.,
761 Werner, M., and Balkanski, Y.: The aerosol-climate model CHAM5-HAM, Atmos. Chem.
762 Phys., 5, 1125-1156,doi: 10.5194/acp-5-1125-2005 2005.
763 Sun, X., Luo, X., Yan, C., Zhen, Z., Xu, J., Zhang, D., Suo, C., and Ding, Y.: Spatio-temporal
764 characteristics of air pollution in Nanjing during 2013 to 2016 under the pollution control and
765 meteorological factors, J. Environ. Earth., 8, 506-515, 2017.
766 Tao, J., Gao, J., Zhang, L., Zhang, R., Che, H., Zhang, Z., Lin, Z., Jing, J., Cao, J., and Hsu, S.
767 C.: $PM_{2.5}$ pollution in a megacity of southwest China: source apportionment and implication,
768 Atmos. Chem. Phys., 14, 8679-8699,doi: 10.5194/acp-14-8679-2014, 2014a.
769 Tao, Y., Yin, Z., Ye, X., Ma, Z., and Chen, J.: Size distribution of water-soluble inorganic ions
770 in urban aerosols in Shanghai, Atmos. Pollut. Res., 5, 639-647, 2014b.
771 Wang, G., Zhang, R., Gomez, M. E., Yang, L., Levy Zamora, M., Hu, M., Lin, Y., Peng, J.,
772 Guo, S., Meng, J., Li, J., Cheng, C., Hu, T., Ren, Y., Wang, Y., Gao, J., Cao, J., An, Z., Zhou,

773 W., Li, G., Wang, J., Tian, P., Marrero-Ortiz, W., Secrest, J., Du, Z., Zheng, J., Shang, D., Zeng,
774 L., Shao, M., Wang, W., Huang, Y., Wang, Y., Zhu, Y., Li, Y., Hu, J., Pan, B., Cai, L., Cheng,
775 Y., Ji, Y., Zhang, F., Rosenfeld, D., Liss, P. S., Duce, R. A., Kolb, C. E., and Molina, M. J.:
776 Persistent sulfate formation from London Fog to Chinese haze, Proc. Natl. Acad. Sci. U.S.A,
777 113, 13630-13635, 2016.
778 Wang, H., Lou, S., Huang, C., Qiao, L., Tang, X., Chen, C., Zeng, L., Wang, Q., Zhou, M., and
779 Lu, S.: Source Profiles of Volatile Organic Compounds from Biomass Burning in Yangtze
780 River Delta, China, Aerosol. Air. Qual. Res., 14, 818–828, 2014.
781 Wang, H., Tian, M., Li, X., Chang, Q., Cao, J., Yang, F., Ma, Y., and He, K.: Chemical
782 Composition and Light Extinction Contribution of $PM_{2.5}$ in Urban Beijing for a 1-Year Period,
783 Aerosol Air Qual. Res, 15, 2200-2211, 2015a.
784 Wang, H. L., Qiao, L. P., Lou, S. R., Zhou, M., Chen, J. M., Wang, Q., Tao, S. K., Chen, C. H.,
785 Huang, H. Y., Li, L., and Huang, C.: $PM_{2.5}$ pollution episode and its contributors from 2011 to
786 2013 in urban Shanghai, China, Atmos. Environ., 123, 298-305, 2015b.
787 Wang, S., Yu, S., Yan, R., Zhang, Q., Li, P., Wang, L., Liu, W., and Zheng, X.: Characteristics
788 and origins of air pollutants in Wuhan, China, based on observations and hybrid receptor
789 models, J. Air Waste Manage. Assoc., 67, 739-753,doi: 10.1080/10962247.2016.1240724,
790 2017.
791 Wang, T., Nie, W., Gao, J., Xue, L. K., Gao, X. M., Wang, X. F., Qiu, J., Poon, C. N., .Meinardi,
792 S., Blake, D., Wang, S. L., Ding, A. J., Chai, F. H., Zhang, Q. Z., and Wang, W. X.: Air quality
793 during the 2008 Beijing Olympics: secondary pollutants and regional impact, Atmos. Chem.
794 Phys., 10, 7603-7615,doi: 10.5194/acp-10-7603-2010, 2010.
795 Wang, X., Bi, X., Sheng, G., and Fu, J.: Hospital indoor $PM_{10}/PM_{2.5}$ and associated trace
796 elements in Guangzhou, China, Sci. Total Environ., 366, 124-135,doi:
797 10.1016/j.scitotenv.2005.09.004, 2006.
798 Wang, X., Miao, Y., Zhang, Y., Li, Y., Wu, M., and Yu, G.: Primary sources and secondary
799 formation of organic aerosols in Beijing, China, Environ. Sci. Technol., 46, 9846-9853, 2012.
800 Wang, Y. Q., Zhang, X. Y., and Draxler, R. R.: TrajStat: GIS-based software that uses various

801 trajectory statistical analysis methods to identify potential sources from long-term air pollution
802 measurement data, Environ. Model. Software, 24, 938-939, 2009.
803 Wei, F., Chen, J., Wu, Y., and Zheng, C.: Study of the background contents of 61 elements of
804 soils in China, Environmental Science, 12, 12-19, 1991
805 Wen, H., and Carignan, J.: Reviews on atmospheric selenium: Emissions, speciation and fate,
806 Atmos. Environ., 41, 7151-7165, 2007.
807 Xiang, L., Lu, X. X., Higgitt, D. L., and Wang, S. M.: Recent lake sedimentation in the middle
808 and lower Yangtze basin inferred from ^{137}Cs and ^{210}Pb measurements, J. Asian Earth Sci., 21,
809 77-86, 2002.
810 Xiao, H., Xiao, H., Luo, L., Shen, C., Long, A., Chen, L., Long, Z., and Li, D.: Atmospheric
811 aerosol compositions over the South China Sea: temporal variability and source apportionment,
812 Atmos. Chem. Phys., 17, 3199-3214,doi: 10.5194/acp-17-3199-2017, 2017.
813 Xu, H., Cao, J., Chow, J. C., Huang, R.-J., Shen, Z., Chen, L. A., Ho, K. F., and Watson, J. G.:
814 Inter-annual variability of wintertime $PM_{2.5}$ chemical composition in Xi'an, China: Evidences
815 of changing source emissions, Sci. Tot. Environ., 545, 546-555, 2016a.
816 Xu, H. M., Cao, J. J., Ho, K. F., Ding, H., Han, Y. M., Wang, G. H., Chow, J. C., Watson, J.
817 G., Khol, S. D., Qiang, J., and Li, W. T.: Lead concentrations in fine particulate matter after the
818 phasing out of leaded gasoline in Xi'an, China, Atmos. Environ., 46, 217-224, 2012.
819 Xu, W. Y., Zhao, C. S., Ran, L., Deng, Z. Z., Liu, P. F., Ma, N., Lin, W. L., Xu, X. B., Yan, P.,
820 He, X., Yu, J., Liang, W. D., and Chen, L. L.: Characteristics of pollutants and their correlation
821 to meteorological conditions at a suburban site in the North China Plain, Atmos. Chem. Phys.,
822 11, 4353-4369,doi: 10.5194/acp-11-4353-2011, 2011.
823 Xu, X., Zhao, T., Liu, F., Gong, S. L., Kristovich, D., Lu, C., Guo, Y., Cheng, X., Wang, Y.,
824 and Ding, G.: Climate modulation of the Tibetan Plateau on haze in China, Atmos. Chem. Phys.,
825 16, 1365-1375,doi: 10.5194/acp-16-1365-2016, 2016b.
826 Zhan, J., Gao, Y., Li, W., Chen, L., Lin, H., and Lin, Q.: Effects of ship emissions on
827 summertime aerosols at Ny–Alesund in the Arctic, Atmos. Pollut. Res., 5, 500-510, 2014.
828 Zhang, F., Chen, Y., Tian, C., Wang, X., Huang, G., Fang, Y., and Zong, Z.: Identification and

quantification of shipping emissions in Bohai Rim, China, Sci. Tot. Environ., 497, 570-577, 2014.

Zhang, F., Wang, Z., Cheng, H., Lv, X., Gong, W., Wang, X., and Zhang, G.: Seasonal variations and chemical characteristics of $PM_{2.5}$ in Wuhan, central China, Sci. Tot. Environ., 518, 97-105, 2015.

Zhang, F., Chen, Y., Tian, C., Lou, D., Li, J., Zhang, G., and Matthias, V.: Emission factors for gaseous and particulate pollutants from offshore diesel engine vessels in China, Atmos. Chem. Phys., 16, 6319-6334,doi: 10.5194/acp-16-6319-2016, 2016.

Zhang, M., Wang, X., Chen, J., Cheng, T., Wang, T., Yang, X., Gong, Y., Geng, F., and Chen, C.: Physical characterization of aerosol particles during the Chinese New Year's firework events, Atmos. Environ., 44, 5191-5198, 2010.

Zhang, R., Jing, J., Tao, J., Hsu, S. C., Wang, G., Cao, J., Lee, C. S. L., Zhu, L., Chen, Z., Zhao, Y., and Shen, Z.: Chemical characterization and source apportionment of $PM_{2.5}$ in Beijing: seasonal perspective, Atmos. Chem. Phys., 13, 7053-7074,doi: 10.5194/acp-13-7053-2013, 2013.

Zhang, X., Zhuang, G., Guo, J., Yin, K., and Zhang, P.: Characterization of aerosol over the Northern South China Sea during two cruises in 2003, Atmos. Environ., 41, 7821-7836, 2007.

Zhao, B., Wang, S. X., Liu, H., Xu, J. Y., Fu, K., Klimont, Z., Hao, J. M., He, K. B., Cofala, J., and Amann, M.: NOx emissions in China: historical trends and future perspectives, Atmos. Chem. Phys., 13, 16047-16112,doi: 10.5194/acp-13-9869-2013, 2013a.

Zhao, M., Zhang, Y., Ma, W., Fu, Q., Yang, X., Li, C., Zhou, B., Yu, Q., and Chen, L.: Characteristics and ship traffic source identification of air pollutants in China's largest port, Atmos. Environ., 64, 277-286, 2013b.

Zhao, P. S., Dong, F., He, D., Zhao, X. J., Zhang, X. L., Zhang, W. Z., Yao, Q., and Liu, H. Y.: Characteristics of concentrations and chemical compositions for $PM_{2.5}$ in the region of Beijing, Tianjin, and Hebei, China, Atmos. Chem. Phys., 13, 4631-4644,doi: 10.5194/acp-13-4631-2013, 2013c.

Zhao, R., Han, B., Lu, B., Zhang, N., Zhu, L., and Bai, Z.: Element composition and source

857 apportionment of atmospheric aerosols over the China Sea, Atmos. Pollut. Res., 6, 191-201,
858 2015.
859 Zhao, X. J., Zhao, P. S., Xu, J., Meng, W., Pu, W. W., Dong, F., He, D., and Shi, Q. F.: Analysis
860 of a winter regional haze event and its formation mechanism in the North China Plain, Atmos.
861 Chem. Phys., 13, 5685-5696,doi: 10.5194/acp-13-5685-2013, 2013d.
862 Zhou, D., Li, B., Huang, X., Virkkula, A., Wu, H., Zhao, Q., Qiao, Y., Shen, G., Ding, A.,
863 Zhang, J., Liu, Q., Li, L., Li, C., Chen, F., and Yuan, S.: The Impacts of Emission Control and
864 Regional Transport on $PM_{2.5}$ Ions and Carbon Components in Nanjing during the 2014 Nanjing
865 Youth Olympic Games, Aerosol. Air. Qual. Res., 17, 730-740,doi: 10.4209/aaqr.2016.03.0131,
866 2017.
867 Zhou, M., Qiao, L., Zhu, S., Li, L., Lou, S., Wang, H., Wang, Q., Tao, S., Huang, C., and Chen,
868 C.: Chemical characteristics of fine particles and their impact on visibility impairment in
869 Shanghai based on a 1-year period observation, J. Environ. Sci. (China), 48, 151-160, 2016.
870 Zou, Y., Deng, X. J., Zhu, D., Gong, D. C., Wang, H., Li, F., Tan, H. B., Deng, T., Mai, B. R.,
871 and Liu, X. T.: Characteristics of 1 year of observational data of VOCs, NOx and O_3 at a
872 suburban site in Guangzhou, China, Atmos. Chem. Phys., 15, 6625-6636,doi: 10.5194/acp-15-
873 6625-2015, 2015.

Atmos. Chem. Phys. Discuss., https://doi.org/10.5194/acp-2018-225
Manuscript under review for journal Atmos. Chem. Phys.
Discussion started: 25 April 2018

Atmospheric Chemistry and Physics Discussions

Captions of Figure and Table

Table 1. The levels of $PM_{2.5}$ and $PM_{1.0}$ sampled during YRC.

Table 2. The pollutant levels and meteorological parameters in eight different episodes.

Table 3. Average concentration of the elements in $PM_{2.5}$ and $PM_{1.0}$ (ng m^{-3}) during YRC

Table 4. Comparisons of trace element concentrations with the reported data (μg m^{-3}).

Figure 1. Cruise tracks, source region limits, the sampling sites and land use during YRC.

Figure 2. (a) aerosol optical depth(AOD); (b) the total CO column mixture ratio; (c) the SO_2 column concentration; (d) the NO_2 column level.

Figure 3. Comparisons major ionic species during YRC with other regions, including: Beijing, Xi'an, Chengdu, Wuhan, Guangzhou, Shanghai, Northern South China Sea, Taiwan Strait, South China Sea, East China Sea and Tuoji Island. The red lines mark the sample routes in different cruises.

Figure 4. Spatial concentration distributions of the soluble ions and levoglucosan in $PM_{2.5}$.

Figure 5. (a) Principle component analysis (PCA) of the typical elements in $PM_{2.5}$; **(b)** Time series of four typical element sources derived from PCA. All of the units are in μg m^{-3}.

Figure 6. Probable sources from PSCF for individual elements in $PM_{2.5}$ during YRC. The criteria are the mean concentration for all.

Figure 7. The primary of ship emission along YRC and number of ship distribution in the Yangtze River channel.

Atmos. Chem. Phys. Discuss., https://doi.org/10.5194/acp-2018-225
Manuscript under review for journal Atmos. Chem. Phys.
Discussion started: 25 April 2018

Atmospheric Chemistry and Physics Discussions

Table 1

Sample Number	Start data UTC	Day/Night Samples	Ship state	Sampling duration	Average Latitude, °N	Average Longitude, °E	$PM_{2.5}$ (μg m^{-3})	$PM_{1.0}$ (μg m^{-3})	$PM_{1.0}/PM_{2.5}$
#1	25-Nov-15	Daily	Moving	24 hours	30.95	117.78	63.83	58.3	91.33%
#2	26-Nov-15	Daily	Moving	24 hours	30.3	116.95	112.7	84.58	75.06%
#3	27-Nov-15	Daily	Moving	24 hours	29.73	115.86	106.4	90.37	84.96%
#4	28-Nov-15	Daily	Moving	24 hours	30.37	115.06	81.49	73.69	90.43%
#5	29-Nov-15	Daytime	Moving	12 hours	30.63	114.53	157.7	136.1	86.32%
#6	29-Nov-15	Nighttime	Stopping	12 hours	30.69	114.45	161.8	152.2	94.06%
#7	30-Nov-15	Daytime	Moving	12 hours	30.42	114.92	80.56	65.56	81.38%
#8	30-Nov-15	Nighttime	Stopping	12 hours	30.09	115.32	106.3	89.29	83.99%
#9	1-Dec-15	Daytime	Moving	12 hours	29.72	115.97	96.0	81.83	85.24%
#10	1-Dec-15	Nighttime	Moving	12 hours	30.32	116.89	92.02	82.86	90.04%
#11	2-Dec-15	Daytime	Moving	12 hours	31.08	117.96	122.8	85.17	69.34%
#12	2-Dec-15	Nighttime	Moving	12 hours	31.9	118.55	163.2	118.4	72.55%
#13	3-Dec-15	Daytime	Moving	12 hours	32.27	119.44	152.9	108.7	71.09%
#14	3-Dec-15	Nighttime	Moving	12 hours	31.95	120.27	133.9	105.6	78.89%
#15	4-Dec-15	Daytime	Moving	12 hours	31.7	121.18	146.1	111.8	76.57%
#16	4-Dec-15	Nighttime	Stopping	12 hours	31.38	121.6	131.2	102.7	78.27%

Atmos. Chem. Phys. Discuss., https://doi.org/10.5194/acp-2018-225
Manuscript under review for journal Atmos. Chem. Phys.
Discussion started: 25 April 2018

Atmospheric Chemistry and Physics Discussions

Table 2

Periods	Data and time (BST[a])	Latitude	Longitude	wind speed (m/s)	RH%	NOx (ppb)	SO_2 (ppb)	CO (ppb)	$PM_{2.5}$ (SN[b])	T/B
EP1	2015/11/22 12:00 to 2015/11/23 18:00	31.28 to 32.22	121.23 to 119.55	3.01	88.95	65.51	6.32	443.91		1.59
EP2	2015/11/25 12:00 to 2015/11/27 14:00	31.01 to 29.91	117.79 to 116.35	2.86	66.73	57.50	12.45	704.48	(#1,2)	0.81
EP3	2015/11/27 14:00 to 2015/11/29 00:00	29.84 to 30.50	116.35 to 114.83	2.48	69.72	68.16	16.15	676.20	(#3,4)	1.20
EP4	2015/11/29 00:00 to 2015/11/30 18:00	30.50 to 30.18	114.83 to 115.25	2.18	83.01	62.65	8.60	1030.25	(#5-7)	0.97
EP5	2015/11/30 18:00 to 2015/12/01 20:00	30.18 to 30.02	115.25 to 116.66	2.32	79.64	51.92	11.66	989.75	(#8,9)	2.61
EP6	2015/12/01 20:00 to 2015/12/02 20:00	30.02 to 31.67	116.66 to 118.40	3.84	74.67	31.00	4.09	1139.33	(10,11)	0.96
EP7	2015/12/02 20:00 to 2015/12/03 20:00	31.67 to 32.32	118.40 to 119.73	5.39	44.91	23.73	7.87	1224.88	(#12,13)	1.00
EP8	2015/12/03 20:00 to 2015/12/05 06:00	32.32 to 31.36	119.73 to 121.61	2.68	38.86	57.55	16.62	1061.46	(#14-16)	1.73

[a] Beijing standard time (GMT-8); T/B is ratio of toluene to benzene; [b] sample number in Table 1.

Atmos. Chem. Phys. Discuss., https://doi.org/10.5194/acp-2018-225
Manuscript under review for journal Atmos. Chem. Phys.
Discussion started: 25 April 2018

Atmospheric Chemistry and Physics Discussions

Table 3

Contents		Average	Max	Min	Median	SD[a]
Mg	$PM_{2.5}$	629.87	1487.67	135.69	589.13	358.57
	$PM_{1.0}$	328.57	699.09	17.26	359.42	213.44
Al	$PM_{2.5}$	863.87	2400.13	21.13	786.17	618.66
	$PM_{1.0}$	631.37	1894.40	100.78	473.46	483.74
K	$PM_{2.5}$	865.88	1723.87	368.51	805.73	367.14
	$PM_{1.0}$	771.80	1560.67	326.41	739.86	303.33
Ca	$PM_{2.5}$	2724.35	5657.60	391.54	2381.94	1729.51
	$PM_{1.0}$	1525.39	3371.73	108.21	1455.19	1108.03
V	$PM_{2.5}$	9.71	60.00	0.19	7.33	13.45
	$PM_{1.0}$	9.20	55.50	1.18	6.80	12.72
Cr	$PM_{2.5}$	22.29	62.67	2.16	16.73	16.51
	$PM_{1.0}$	21.67	48.17	2.67	22.74	13.31
Mn	$PM_{2.5}$	56.63	152.12	9.08	42.56	43.42
	$PM_{1.0}$	45.80	106.33	8.58	31.56	31.75
Fe	$PM_{2.5}$	1644.84	5188.18	38.87	860.40	1590.29
	$PM_{1.0}$	934.30	2616.83	46.74	516.37	850.12
Co	$PM_{2.5}$	0.82	2.88	0.00	0.48	0.75
	$PM_{1.0}$	0.62	1.67	0.07	0.26	0.53
Ni	$PM_{2.5}$	10.53	73.64	1.83	5.61	16.82
	$PM_{1.0}$	8.19	32.29	1.39	4.35	7.89
Cu	$PM_{2.5}$	18.79	49.87	4.07	17.66	11.28
	$PM_{1.0}$	15.21	37.07	3.70	12.32	7.87
Zn	$PM_{2.5}$	295.08	638.08	125.36	221.83	159.05
	$PM_{1.0}$	288.84	485.26	81.91	261.06	156.34
As	$PM_{2.5}$	37.33	107.17	0.87	31.50	28.14
	$PM_{1.0}$	41.73	111.85	12.46	30.70	32.00
Se	$PM_{2.5}$	6.08	12.18	2.70	5.78	2.57
	$PM_{1.0}$	6.48	11.04	3.07	6.40	2.76
Cd	$PM_{2.5}$	2.72	5.00	1.30	2.50	1.06
	$PM_{1.0}$	5.42	39.20	1.30	3.33	9.09
Tl	$PM_{2.5}$	0.32	0.90	0.00	0.29	0.22
	$PM_{1.0}$	0.41	0.89	0.14	0.35	0.23
Pb	$PM_{2.5}$	98.37	176.54	53.26	95.68	35.91
	$PM_{1.0}$	110.45	274.80	53.04	102.84	54.07

[a] SD is one standard deviation.

Atmos. Chem. Phys. Discuss., https://doi.org/10.5194/acp-2018-225
Manuscript under review for journal Atmos. Chem. Phys.
Discussion started: 25 April 2018

Atmospheric Chemistry and Physics Discussions

Table 4

	2015[a]	2003	2011	2013-2014	2012-2013	2011	2012-2013	2008-2009	2009-2010
	(this study)	(Zhang et al., 2007)	(Zhao et al., 2015)	(Li et al., 2016)	(Lai et al., 2016)	(Tao et al., 2014)	(Zhang et al., 2015)	(Huang et al., 2013)	(Zhao et al., 2013)
	Winter	Spring	Spring	Winter	Winter	Winter	Winter	Winter	Winter
	Yangtze river channel[b]	Northern South China Sea	East China sea	Taiwan strait	Guangzhou (rural)	Chengdu	Wuhan	Shanghai	Beijing
Al	0.86	0.31	3.28	3.00	0.21	0.43	—	0.64	1.03
Ca	2.72	0.82	2.40	2.00	0.11	0.26	2.27	0.72	1.85
Fe	1.64	0.32	1.37	1.30	0.16	0.61	1.42	0.56	1.55
Mg	0.63	0.11	0.83	2.40	2.30	0.16	0.61	0.26	0.57
As	0.04	—	0.01	—	—	0.02	0.04	0.02	0.01
Cd	0.00	—	—	—	—	0.00	0.01	—	—
Cr	0.02	0.03	—	0.60	—	0.01	0.01	0.02	0.01
Cu	0.02	—	0.01	—	0.03	0.03	0.03	0.04	0.04
Mn	0.06	—	0.01	0.70	0.03	0.07	0.13	0.04	0.09
Ni	0.01	—	0.01	0.90	—	0.00	0.01	0.01	0.01
Pb	0.10	0.16	0.02	0.70	0.09	0.20	0.24	0.06	0.15
V	0.01	—	0.02	—	—	0.00	—	0.01	—
Zn	0.30	—	0.07	0.60	0.27	0.32	0.37	0.13	0.30

[a] Sampling periods; [b] Sampling sites

Atmos. Chem. Phys. Discuss., https://doi.org/10.5194/acp-2018-225
Manuscript under review for journal Atmos. Chem. Phys.
Discussion started: 25 April 2018

Atmospheric Chemistry and Physics Discussions

Figure 1.

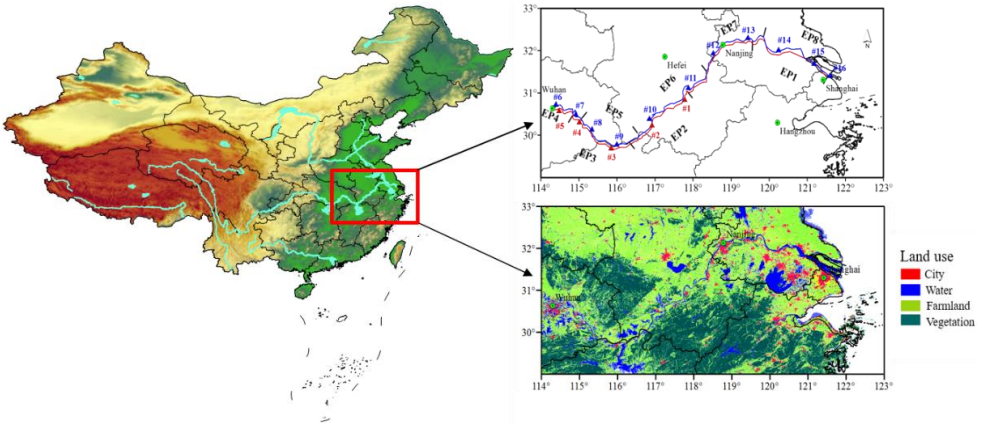

Atmos. Chem. Phys. Discuss., https://doi.org/10.5194/acp-2018-225
Manuscript under review for journal Atmos. Chem. Phys.
Discussion started: 25 April 2018

Atmospheric Chemistry and Physics Discussions

Figure 2.

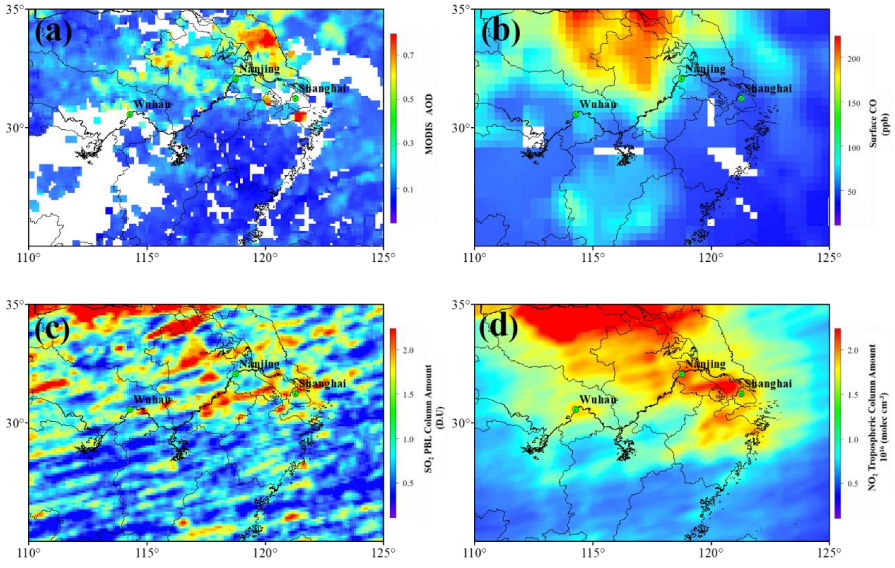

Atmos. Chem. Phys. Discuss., https://doi.org/10.5194/acp-2018-225
Manuscript under review for journal Atmos. Chem. Phys.
Discussion started: 25 April 2018

Atmospheric Chemistry and Physics Discussions

Figure 3.

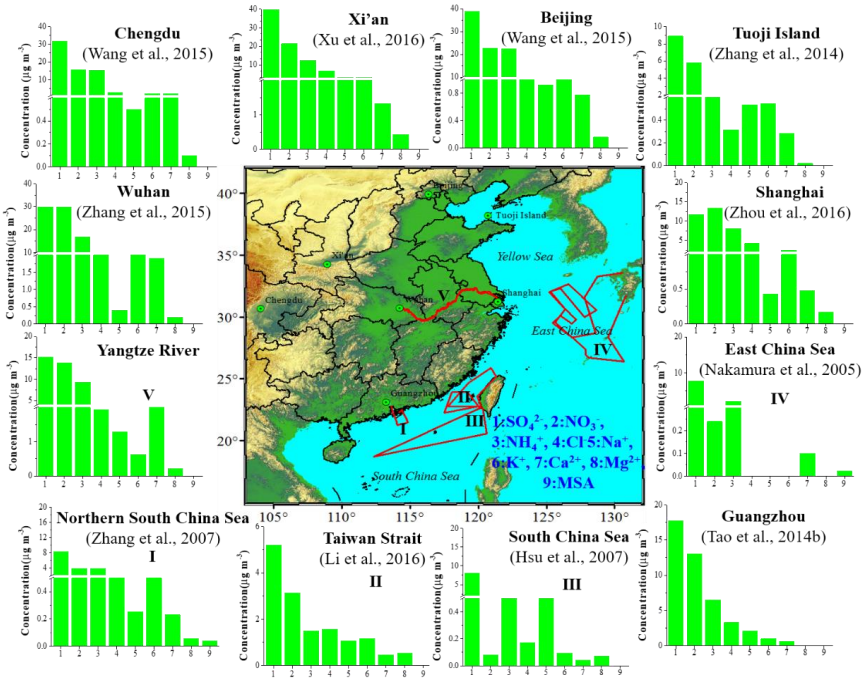

Atmos. Chem. Phys. Discuss., https://doi.org/10.5194/acp-2018-225
Manuscript under review for journal Atmos. Chem. Phys.
Discussion started: 25 April 2018

Atmospheric Chemistry and Physics Discussions

Figure 4.

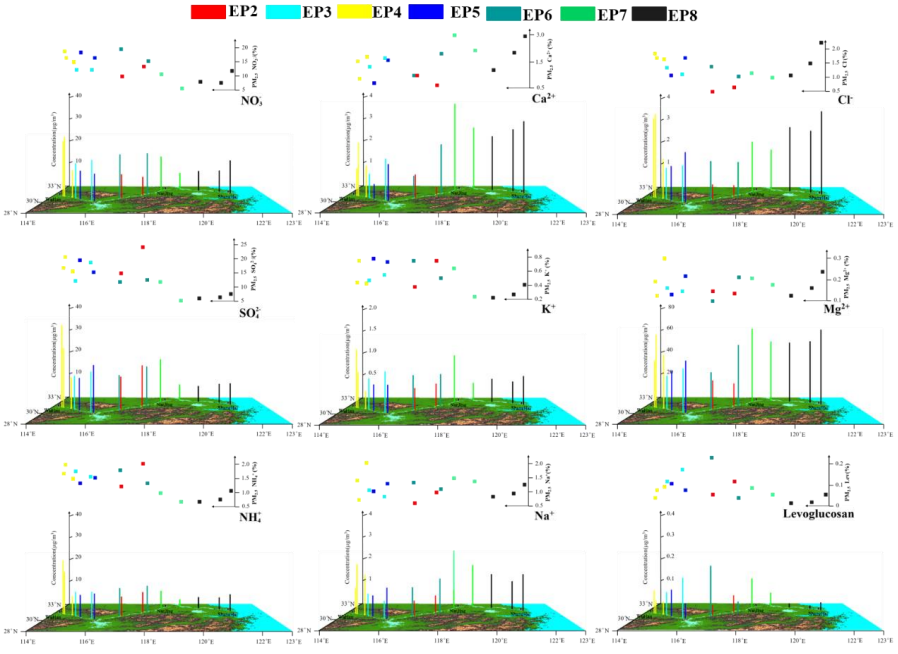

Atmos. Chem. Phys. Discuss., https://doi.org/10.5194/acp-2018-225
Manuscript under review for journal Atmos. Chem. Phys.
Discussion started: 25 April 2018

Atmospheric Chemistry and Physics Discussions

Figure 5.

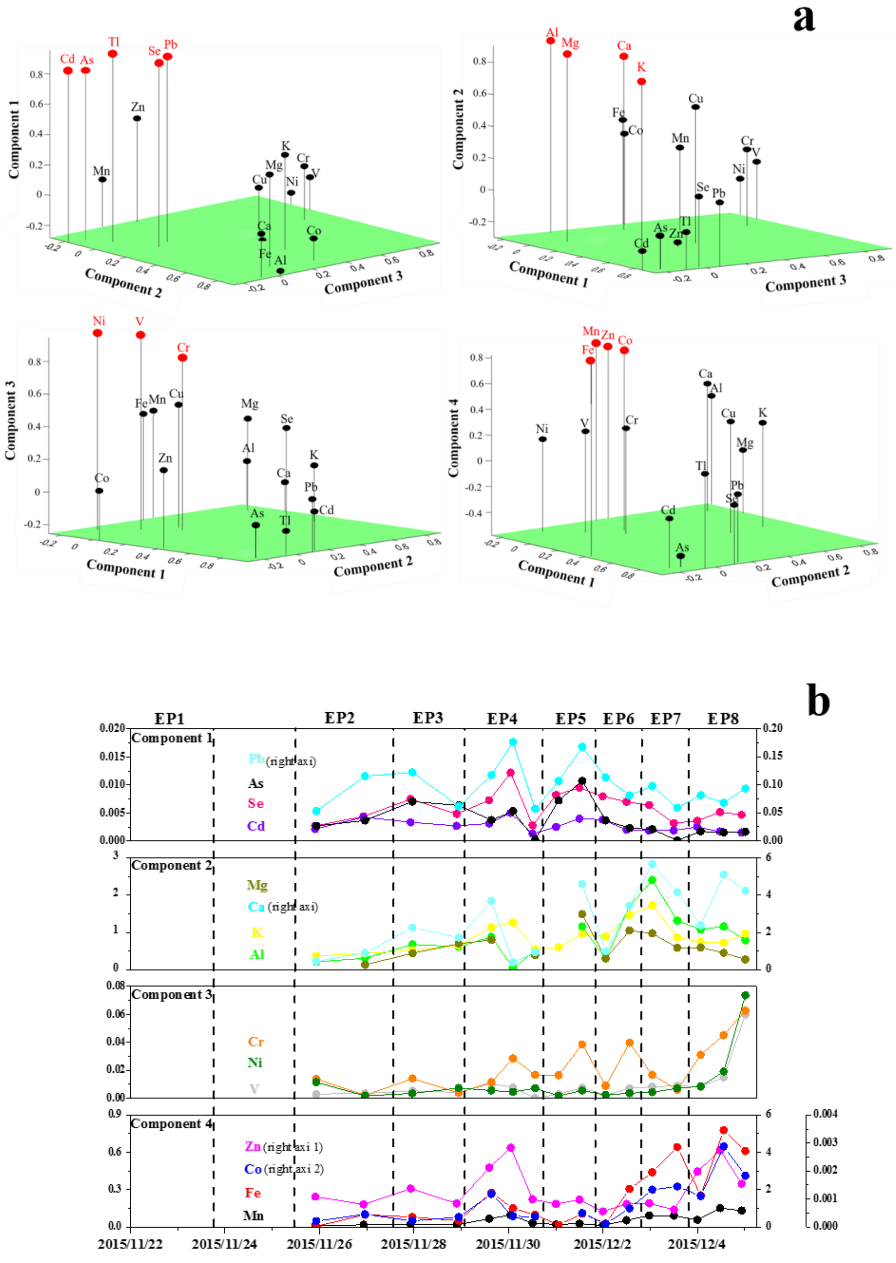

Atmos. Chem. Phys. Discuss., https://doi.org/10.5194/acp-2018-225
Manuscript under review for journal Atmos. Chem. Phys.
Discussion started: 25 April 2018

Atmospheric Chemistry and Physics Discussions

Figure 6.

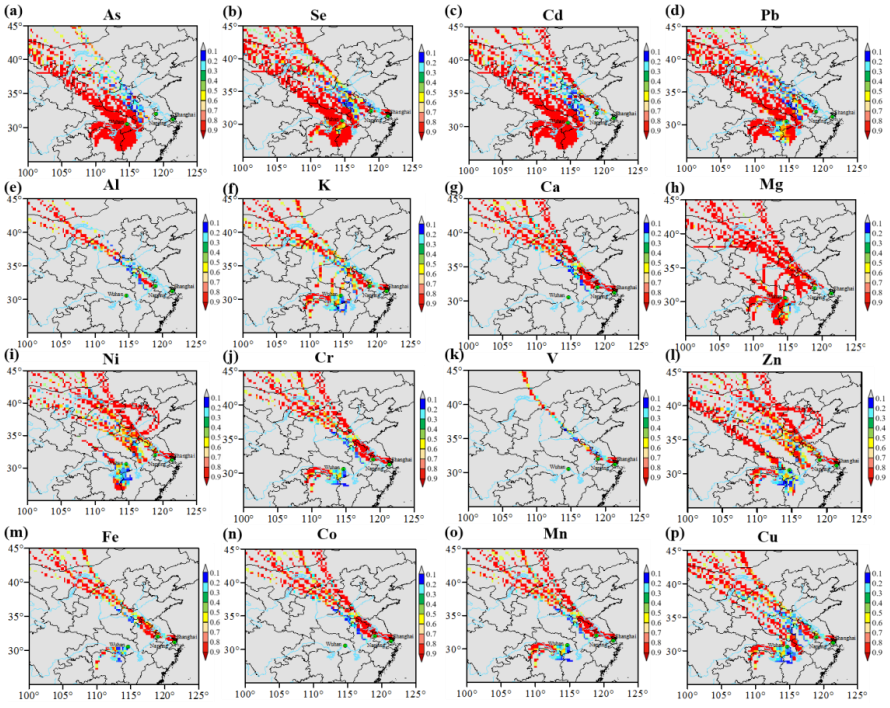

Atmos. Chem. Phys. Discuss., https://doi.org/10.5194/acp-2018-225
Manuscript under review for journal Atmos. Chem. Phys.
Discussion started: 25 April 2018

Atmospheric Chemistry and Physics Discussions

Figure 7.